

Elsevier Editorial System(tm) for Nuclear Inst. and Methods in Physics Research, A  
Manuscript Draft

Manuscript Number: NIMA-D-08-00031R1

Title: Extended-time-scale creep measurement on Maraging cantilever blade springs.

Article Type: Research Paper

Section/Category: Special Applications

Keywords: maraging; creep; Young's modulus thermal variation; Arrhenius acceleration; seismic isolation

Corresponding Author: Miss Nicole Virdone,

Corresponding Author's Institution: California Institute of Technology

First Author: Nicole K Virdone

Order of Authors: Nicole K Virdone; Juri Agresti; Alessandro Bertolini; Riccardo DeSalvo; Rosalia Stellacci; Justin Kamp; Maddalena Mantovani; Virginio Sannibale; Marco Tarallo; Lisa Kaltenegger

Manuscript Region of Origin:

**Abstract:** Two controlled temperature facilities were built to induce an accelerated creep rate in a Maraging steel GAS spring and to measure the material's creep over an artificially extended period of time. The data acquisition of the first experiment lasted for almost a year, but then the blades were allowed to creep for six more years before measuring the permanent deformation integrated over time. The data from this first experiment was polluted by a defect in the data acquisition software, but yielded overall creep limits and an evaluation of the Arrhenius acceleration of creep speed with temperature ( $1.28 \pm 0.13 / \text{oC}$ ). The duration of the second experiment was only one year but more free of systematic errors. The effective test period of this second experiment (normalized with the Arrhenius acceleration measured in the first experiment) extends in the billions of years showing no sign of anomalous creep. The result of both experiments also produced a simple procedure capable of eliminating all practical effects of creep from the Advanced LIGO seismic isolation and suspensions. Measurements of creep under various stress levels, and of the thermal variations of Young's modulus ( $2.023 (\pm 0.013) 10^{-4} / \text{oC}$ ) are reported as well.



May 20, 2008

Dear Dr. Barletta and fellow editors,

A revised version of the "Extended-time-scale creep measurement on Maraging cantilever blade springs" has been uploaded to Elsevier. Thank you for all of the useful comments. Each comment in the previous email was reviewed point by point and revised as suggested with the following exceptions and rebuttles:

- In response to point 2, the formula is the Arrhenius thermal acceleration mentioned just above, we find it superfluous to repeat it in the introduction.
- In response to point 3, The key point in showing both graphs is to illustrate how the measurements are upper limits, still dominated by the systematics of the correction factors and compatible to zero. Note that applying our best estimated corrections the creep is actually negative (positive slope), which is obviously impossible but makes our claim of zero creep much more compelling. Also note that the raw measurement is only 1.1 standard deviations from zero, and the corrected one 1.5 standard deviations, but in the impossible direction.
- We believe that our claim that the creep is compatible to zero within our errors is a reasonable claim. Following your comment, though, we modified the caption from

"The fits in the two curves,  $-0.11 \pm 0.1$  mm/day for the raw data and  $0.15 \pm 0.1$  mm/day for the corrected data are both compatible, within our measurement errors, with no creep. "

to:

"The fits in the two curves,  $-0.11 \pm 0.1$  mm/day for the raw data and  $0.15 \pm 0.1$  mm/day for the corrected data are both compatible, within our measurement errors, with no creep. The opposite sign of the two slopes indicated that the measurement is dominated by systematics."

We worked on all other (very useful) comments. Hopefully the new version will be agreeable to the referees.

Sincerely,

Nicole Virdone

Email: [nvirdone@ucla.edu](mailto:nvirdone@ucla.edu)

Phone: 626-379-0873

1 **Extended-time-scale creep measurement on Maraging cantilever blade springs.**

2

3 Nicole Virdone[1,2], Juri Agresti[2,3], Alessandro Bertolini [7], Riccardo DeSalvo[2],

4 Rosalia Stellacci [2,3,5], Justin Kamp [6], Maddalena Mantovani[2,3,4], Virginio

5 Sannibale[2], Marco Tarallo[2,3], Lisa Kaltenegger [8]

6

7 1 Mayfield Senior High School, 500 Bellefontaine St, Pasadena, CA 91105-USA,

8 now at University of California - Los Angeles, 405 Hilgard Ave, Los Angeles, CA

9 90095-USA

10 2 LIGO Observatories, California Institute of Technology, Pasadena, CA 91125-USA

11 3 Dipartimento di Fisica "Enrico Fermi" and INFN Sezione di Pisa, Università di Pisa,

12 Largo Bruno Pontecorvo, I-56127 Pisa, Italy

13 4 now at Università di Siena, dipartimento di Fisica - Via Roma, 56, I-53100Siena, Italy

14 5 now at Università degli Studi di Napoli Federico II - Corso Umberto I, I-80138 Napoli,

15 Italy

16 6 now at Chalmers University of Technology, SE-412 96 Goteborg, Sweden

17 7 now at DESY, Forschung Linear Collider Division, Notkestrasse 85, D-22607

18 Hamburg, Germany

19 8 now at Harvard Smithsonian Institute for Astrophysics (CfA), 60 Garden Street,

20 Cambridge, MA 02138

21

22 Send Proofs to:

23 Nicole Virdone

1 Postal Address: 415 Gayley Ave. Apt. 105; Los Angeles, CA 90024

2 Phone: (626) 379-0873

3 Email: nvirdone@ucla.edu; nvirdone@gmail.com

4

5 **Abstract**

6

7 Two controlled temperature facilities were built to induce an accelerated creep rate in a  
8 Maraging steel GAS spring and to measure the material's creep over an artificially  
9 extended period of time. The data acquisition of the first experiment lasted for almost a  
10 year, but then the blades were allowed to creep for six more years before measuring the  
11 permanent deformation integrated over time. The data from this first experiment was  
12 polluted by a defect in the data acquisition software, but yielded overall creep limits and  
13 an evaluation of the Arrhenius acceleration of creep speed with temperature  
14 ( $1.28 \pm 0.13 / ^\circ\text{C}$ ). The duration of the second experiment was only one year but more free  
15 of systematic errors. The effective test period of this second experiment (normalized  
16 with the Arrhenius acceleration measured in the first experiment) extends in the billions  
17 of years showing no sign of anomalous creep. The result of both experiments also  
18 produced a simple procedure capable of eliminating all practical effects of creep from the  
19 Advanced LIGO seismic isolation and suspensions. Measurements of creep under  
20 various stress levels, and of the thermal variations of Young's modulus ( $2.023 (\pm 0.013)$   
21  $10^{-4} / ^\circ\text{C}$ ) are reported as well.

22

23 Classification codes:

1 62.20.Hg Creep

2 61.72.Hh Indirect evidence of dislocations and other defects (resistivity, slip, creep,

3 strains, internal friction, EPR, NMR, etc.)

4 62.20.de Elastic moduli

5 62.20.fq Plasticity and superplasticity

6

7 Key Words:

8 Maraging; creep; Young's modulus thermal variation; Arrhenius acceleration; seismic

9 isolation

10

11 **Footnotes**

12

13 Conversely, if creep was to completely relax the radial compression without changing

14 the energy stored in the bending that is holding up the load, only the resonant frequency

15 would be changed and not the vertical equilibrium position.

16 <sup>2</sup> The linear droop of an unconstrained blade can be obtained by rescaling the measured

17 droop with the square of ratio of the resonant frequencies times a small correction factor

18 of the order of one. Considering that we have observed that changing the radial

19 compression does not change the vertical equilibrium point, one can estimate this

20 correction factor to be very close to unity.

21 <sup>3</sup> Of course any real-life creep relieving procedure would be designed to maintain the

22 metal well below the plastic transition and thus avoid any danger of plastic slippage.

1 **1. Introduction**

2

3 All material under stress experiences a measurable creep, which is an increase of its  
4 strain over time. Creep is normally a very slow process involving movement of  
5 dislocations inside the material's grains. Its effect on springs supporting a load is to  
6 reduce the "lifting" power of the spring over time and allow its payload to droop. The  
7 main source of creep is the dislocations' movement, which is normally impeded by the  
8 anchoring of dislocations to other discontinuities of the crystalline matrix. Some  
9 dislocations get freed by local fluctuations of thermal energy, drift down the stress field  
10 until they encounter the next obstacle, and thus generate creep. Dislocation activation is  
11 therefore most likely to occur at higher temperatures following the Arrhenius law. In the  
12 absence of dislocation regeneration, creep is generated using up the available  
13 dislocations. As a consequence, the creep behavior at a constant temperature is expected  
14 to be logarithmic with time, while if the temperature rises, the creep simply accelerates  
15 according to the Arrhenius law [1].

16 If the temperature is increased excessively, new dislocations may appear or become  
17 activated and the creep behavior changes, normally switching from logarithmic to linear.

18

19 All Gravitational Wave interferometers use or propose to use chains of cantilever blade  
20 springs to support the mirror test masses and isolate them from seismic noise. All, to  
21 some level, are affected by creep problems. In Ad-LIGO, blade-springs are made with a  
22 metal alloy called Maraging steel, which has particularly good creep characteristics [2].

1 We made two experiments to characterize the creep in Maraging steel. In both cases we  
2 used temperature to accelerate the creep speed. The first experiment was performed with  
3 unconstrained cantilever blades, each loaded with a free hanging ballast mass and read-  
4 out with a Linear Variable Differential Transformer (LVDT) position transducer. The  
5 blades were attached to the sides of a column, housed in a large oven with a thermal  
6 stabilization of 10 mK/week.

7 In the second test we took advantage of the Geometric Anti Spring (GAS) configuration  
8 to cancel the restoring forces and thus enhance the effects of creep.

9 The GAS filters, initially developed for use in Advanced LIGO [3,4,5], are one of the  
10 most efficient vertical seismic noise attenuation systems. Conceptually similar to  
11 VIRGO's magnetic anti-spring filters [6], they use a symmetric arrangement of strong,  
12 contrapposed, triangular cantilever blades to form a system where the spring restoring  
13 forces can be reduced or even cancelled at will (Figure 1).

14

15 Figure 1: Figure 1 Schematic diagram of the experimental setup.

16 A: Arrangement of a TAMA-SAS GAS spring inside its oven in the measurements  
17 described in chapter 2.

18 The two arcs represent the two opposed cantilever springs. Changing their radial  
19 compression allows tuning of the vertical resonant frequency. The position sensor is  
20 solidly attached to the oven base, and reads the position of a "flag" bolted to the solid  
21 wire that suspends the load. The filter sits on pillars, also resting on the oven base and  
22 traversing the oven thermal insulation. Their thermal expansion is almost exactly  
23 counterbalanced by the thermal expansion of the load suspension wire, which experience



1 the same thermal gradient and has almost identical thermal expansion coefficient. Two  
2 blades at  $180^\circ$  are shown in the graph to facilitate the reader's understanding. In the  
3 experiment a GAS spring with three blades at  $120^\circ$  was used.

4 B: One of the 12 triangular blades mounted around a central pier in the measurements  
5 described in chapter 2.

6 The blades are clamped at  $45^\circ$  on a vertical support plate, and loaded until their tip is  
7 horizontal; the receiver part of an LVDT is mounted on it. A shelf, also attached to the  
8 support plate carries the emitter part of the LVDT. A screw allows the zeroing of the  
9 LVDT at the beginning of the measurement. The structure formed by the pier and the 12  
10 blades is enclosed inside a forced-circulation, thermally controlled walk-in oven.

11

12 The cantilever blades of a GAS filter are originally flat and bend under load. They are  
13 linked to a central keystone, or load disk, and are subject to radial compression. All  
14 radial forces cancel out by symmetry. The dimensioning of the blades is chosen to  
15 support the desired payload at the point of maximal radial compression.

16 Any deviation from that working point results in a reduction of compressional energy, in  
17 its turn resulting in a force proportional to the displacement, just as in a normal spring,  
18 but with the opposite sign (anti-spring).

19 Tuning the blades' radial compression changes the anti-spring strength. This can be done  
20 to null the vertical stiffness of the blades, giving the GAS system its "soft spring"  
21 qualities without changing the vertical force supporting the payload. The blade's profile  
22 is chosen so that a constant stress is imposed anywhere along the blades. The filter can

1 be sized to lift any payload, imposing any arbitrary stress in the material, and obtaining  
2 any vertical spring stiffness (vertical resonant frequency) all at the same time.

3

4 The GAS configuration, which is designed to reduce the resonant frequency of vertical  
5 oscillators, is ideal to study creep properties of materials because of its tunable stiffness  
6 and uniform stress in the material. The restoring force cancellation of the GAS  
7 mechanism results in tunable sensitivity to the creep effects (and with the same  
8 amplification factor, to the effects of hysteresis and thermal variations of the Young's  
9 modulus), while the full spring lift capabilities are maintained. The visibility of these  
10 effects is enhanced by the square of the resonant frequency reduction factor [7]. The GAS  
11 springs are particularly well suited for this kind of test because they have, by design,  
12 uniform stress throughout the entire blade surfaces (the profile of the blades is carefully  
13 calculated to produce constant radius of curvature (stress) along the entire blade length  
14 [8]) without increasing the overall stress applied on the spring material.

15 In a vertical oscillator made of normal (unconstrained) springs the energy is periodically  
16 exchanged between gravitational and elastic potential energy at the two end points of the  
17 excursion, via the kinetic energy.

18 In the GAS spring oscillator, a fraction of what would be kinetic energy is stored in a  
19 mechanical potential energy reservoir (the variation of radial compression) largely  
20 independent from the one storing the energy of the vertical movement. This reservoir  
21 stores a very small fraction (few percent) of the overall elastic potential energy. Since the  
22 lift is obtained by integration along the blade length of the stress relative to the vertical  
23 bending (the radial compression does not contribute to the lift), only the creep of the

1 stress of the material contributing to the vertical force can be expected to count in  
2 lowering the payload<sup>1</sup>. Since the vertical component of the stress is the same as in an  
3 unconstrained blade, the GAS principle cannot be expected to significantly change the  
4 amount of energy lost in creep and, while the droop is greatly amplified, the creep-  
5 induced loss of lifting power, measured in Newton, is substantially the same as would be  
6 in an unconstrained cantilever spring under the same load and stress<sup>2</sup>. Therefore the  
7 measurements reported in this paper remain valid for any spring configuration made with  
8 similarly hardened Maraging steel.

9 To make a representative test, creep was measured with a geometry (and stress level)  
10 identical to the spring used in the SAS systems in TAMA (680 MPa) and in the seismic  
11 attenuation system developed for Advanced LIGO [9]. This stress level is also similar to  
12 the stress level used in the LIGO multiple pendulums, i.e. of the order 800 to 1000 MPa.  
13 The thickness of the blade is 2.25mm and the radius of curvature is 240mm. The peak  
14 strain level in the blades of the filter we tested is 0.0047.

15

16 Since creep is generated by thermal fluctuations, it occurs in a shorter time frame at  
17 higher temperatures following an Arrhenius exponential law. The ensuing raise in the  
18 creep rate at higher temperatures is equivalent to an acceleration of time. To calculate the  
19 time acceleration, we conservatively assumed an Arrhenius thermal acceleration of the

---

<sup>1</sup> Conversely, if creep was to completely relax the radial compression without changing the energy stored in the bending that is holding up the load, only the resonant frequency would be changed and not the vertical equilibrium position.

<sup>2</sup> The linear droop of an unconstrained blade can be obtained by rescaling the measured droop with the square of ratio of the resonant frequencies times a small correction factor of the order of one. Considering that we have observed that changing the radial compression does not change the vertical equilibrium point, one can estimate this correction factor to be very close to unity.

1 creep rate of  $\sim 1.175 / ^\circ\text{C}$  (which is close to the lower limit of our acceleration  
2 measurements). The estimation of this acceleration is discussed in Section 5. Although  
3 this number is not very well measured, its actual value is only marginally important for  
4 the development of a procedure to eliminate, to all practical purposes, the ill effects of  
5 creep. Baking the structure under its nominal stress at moderate temperatures allows for  
6 an effective ageing equivalent to very long time periods. With the assumed time  
7 acceleration value, and a heating at only  $150^\circ\text{C}$ , we calculated that the creep speed  
8 increases by a factor of at least  $8.8 \times 10^8$  (see Section 5). Thus at  $150^\circ\text{C}$ , the creep  
9 measured in a day corresponds to what it would experience in 2.4 million years.

10 The most important result is the accelerated burnout of the dislocations that would have  
11 moved over the expanded time frame, and thus a drastic reduction of any further droop  
12 after the specified heat process.

13 Of course if the temperature were raised beyond a certain threshold, other effects  
14 inducing plasticity (new dislocations) would start.

15 The onset of any of these processes would be signaled by a marked increase of creep and  
16 the appearance of a constant creep speed (or even growing with time). Cobalt, Nickel  
17 and Titanium precipitates, interspersed within the martensitic structure of the material  
18 grains, pin down the dislocations in Maraging. When exceeding the elasticity limit, the  
19 dislocations are expected to simply jump over the precipitates that pinned them. As these  
20 precipitates are all statistically equal, the transition is expected to be sharp. After  
21 exceeding the elasticity limit, Maraging is expected to transition to a completely plastic  
22 material [10].

1 The sharp beginning of such a runaway creep was observed, at our stress levels, between  
2 190 and 200°C, detected by monitoring the creep speed while increasing the temperature.  
3 Having identified the stress and temperature levels that induce runaway creep, controlled  
4 baking procedures of the blades under nominal stress can be designed to eliminate all  
5 practical effects of creep.

6 For any Arrhenius creep acceleration rate within the limits measured in Section 5, the  
7 exponential increase of creep speed ensures that, to all practical purposes, all available  
8 dislocations can be burned out and creep stopped, with bake out periods of the order of a  
9 few days at temperatures only ~100°C above room temperatures and without changing  
10 the spring's characteristics.

11 These bakeout conditions are similar and compatible to that recommended for standard  
12 Ultra-High Vacuum bakeout procedures.

13

## 14 **2. Materials and Method**

15

16 We built two creep measurement setups. The first one, built in the year 2000, is  
17 described in Section 4. The second was built in 2004 and is described below.

18 An oven withstanding temperatures up to 200° C was built to house a 60 cm diameter  
19 TAMA-SAS GAS filter [11].

20 A 5-10 mm thick aluminum inner lining of the oven ensured good thermal uniformity. An  
21 air gap of at least 1cm thickness was allowed all around between the filter and the oven  
22 inner lining. A heating tape wrapped around the oven's inner lining and controlled by a  
23 PID temperature controller was used to stabilize the oven temperature at the desired

1 temperature within a fraction of a degree Celsius. The feedback thermocouple was  
2 suspended in air, inside the oven volume. Control thermometers were hooked directly on  
3 the surface of a blade and outside of the oven. The GAS filter, consisting of a three-blade  
4 unit, was tuned to 0.86 Hz (effective elastic constant  $K_{\text{eff}} = 2200 \text{ N/m}$ , a very moderate  
5 GAS tuning). The stainless steel filter frame, with virtually the same thermal expansion  
6 coefficient of the Maraging blades, practically eliminated all differential thermal  
7 expansion effects. A small hole at the bottom of the oven allowed the passage of the wire  
8 supporting the external  $63.7 \pm 0.2 \text{ kg}$  payload. Care was taken so that the wire had a  
9 clearance of about 1 mm in all directions. A 5 cm thick, semi-rigid high-thermal-  
10 insulation foam jacket, precision cut and held by an external steel lining, allowed for no  
11 air circulation between the inside and the outside of the oven. The filter body was  
12 supported through rigid, thin-wall stainless steel pipe spacers running between the filter  
13 body and the inner lining, as well as across the thermal insulation jacket.

14 An external mechanical gauge was connected to the wire to measure the relative height of  
15 the payload with respect to the support of the filter body [12]. Proper care was taken to  
16 ensure that the gauge was not exposed, or in any way affected by the internal temperature  
17 of the oven. The droop of the payload can be easily measured with this gauge to a  
18 precision of  $10 \mu\text{m}$ . We used a mechanical gauge because of its simplicity, while  
19 providing an absolute measurement of the payload droop. The main disadvantage of a  
20 mechanical gauge was the noise introduced by its sticks and slip friction, which is  
21 significant against the softness of the filter.

22 Measurements were performed by manually exciting the vertical oscillation of the spring  
23 and recording the end position read by the gauge. If multiple measurements are graphed

1 in a histogram, the stick and slip of the mechanical gear in the gauge produce a  
2 characteristic double peak distribution (Figure 2) corresponding to whichever direction,  
3 up or down, the movement stopped. This noise can be mitigated by performing many  
4 measurements (typically 60) at a specific time, thus averaging out the systematic error  
5 introduced by the stick and slip bi-stability to acceptable levels (10-20  $\mu\text{m}$ ). This  
6 procedure also eliminates all material hysteresis effects encountered in static  
7 measurements (see discussion of data of Figure 12 in Section 5).

8

9 Figure 2: Typical double horn structure of a vertical position measurement.

10

11 To characterize the temperature behavior of the system, the oven was first heated to  
12 30°C, then up to 40°C, and finally back down to 30°C. During this initial series, the  
13 vertical height of the payload was measured many times per day for a week at both  
14 temperature levels. In Section 6, our measurements showed that the Young modulus of  
15 the blades decreases by  $\sim 2 \times 10^{-4}/^\circ\text{C}$ . This large effect is rapid (several hours of  
16 thermalization; also see the discussion of Figure 11 in Section 6) as compared with the  
17 observed creep times ( $\sim$ days) and fully reversible. Due to its reversibility, it can be  
18 subtracted from the creep effect by simply returning to an original, lower temperature  
19 level after each period at higher temperature. Unfortunately this effect also masks the  
20 instantaneous change of creep slope induced by temperature variations that would  
21 otherwise allow precise measurement of the Arrhenius rate of creep acceleration. The  
22 measurements of thermal variation of the Arrhenius creep rate acceleration and of the  
23 Young's modulus are detailed in Sections 5 and 6 respectively.

1 After the starting measurements between 30 and 40°C, we adopted a baseline temperature  
2 of 40°C for the rest of the experiment. We chose this temperature because it is  
3 sufficiently above room temperature and allows for rapid returns and for stable oven  
4 temperature controls. We then took measurements at monotonically increasing  
5 temperature levels, each followed by a return to the 40°C baseline level. At each  
6 temperature level, daily creep measurements were taken over (typically) two-week  
7 periods, followed by a week of measurements at the baseline temperature of 40°C. Each  
8 daily measurement consisted of about 60 individual position measurements averaged to  
9 mitigate the stick and slip measurement error. The temperature levels we examined are  
10 listed in Table 1.

11 At the end we performed a final, long measurement, at the 40°C baseline temperature. In  
12 the final run, the measurements were taken only twice a week but for a much longer  
13 period of time (118 days) to verify the elimination of creep (within the measurement  
14 sensitivity) expected from our process.

15 It should be noted that every time we increased the temperature, the GAS blades rapidly  
16 relaxed due to the  $\sim 2.023 \times 10^{-4}/^{\circ}\text{C}$  change of Young's modulus. In order to maintain  
17 the GAS filter near its working point, and at as closely as possible a constant strain level,  
18 in the measurements above 90°C we removed some weight from the payload, and  
19 carefully replaced it when returning to the baseline 40°C. This procedure maintained, to  
20 all practical purposes, a constant strain level on the blades and did not affect the  
21 measurement of the absolute value of the creep within each temperature cycle.

22

### 23 **3. Creep Measurement Results**



1

2 The initial creep at each temperature level is mostly masked by the movements generated  
3 by the thermal Young's modulus variations. Thermalization is limited to the first hours  
4 after each temperature change. The manual readout of this setup is not well suited to  
5 follow it and, after the kickoff measurements illustrated in Figure 3, we did not even try  
6 to track it. Each measurement at high temperature shows the initial drop due to the  
7 change of Young's modulus, followed by the logarithmic droop. A measurement  
8 (excluding the initial transient) is shown in Figure 4. The aim of these measurements is  
9 to verify that a creep saturation level is reached (the logarithmic creep dropped below the  
10 measurement sensitivity), and that no macroscopic slope (plasticity) is appearing. The  
11 duration of each step at a specific temperature is also carefully recorded. The  
12 measurement back to the 40°C baseline (Figure 3) is used to measure the creep integrated  
13 over the preceding "at temperature" period while eliminating the effects of the thermal  
14 changes of Young's modulus.

15

16 Figure 3: Typical transient at a temperature change (returning to 40°C). The undershoot  
17 is attributed to thermal variations of the Young's modulus induced by oven temperature  
18 fluctuation before the PID controller stabilizes the temperature, and to differential heating  
19 of the parts. The oven response is slower in descending temperature steps.

20

21 Figure 4: Creep behavior observed at 90°C. The initial creep, masked by the droop  
22 caused by the thermal variations of Young's modulus, is missed in this measurement.

23

1 Occasionally unexplained steps were observed (Figure 5). If they were stress related, the  
2 slippage would only be downward. As we observed steps in both directions we attributed  
3 them to some bistability of our support setup. These unphysical steps are the largest  
4 limiting factor of these measurements.

5  
6 Figure 5: Two unexpected large readout position jumps,  $\sim 100 \mu\text{m}$  downwards observed  
7 on day 12 at  $40^\circ\text{C}$  (left graph) and  $\sim 70 \mu\text{m}$  upwards observed on day 27 at  $60^\circ\text{C}$ . These  
8 jumps were attributed to some external structure bi-stability. The observed jumps are  
9 significantly smaller than the observed creep, and represent our largest experimental  
10 uncertainty.

11  
12 For most of the observed temperature levels, the data closely followed the logarithmic  
13 decay. A progressive droop, adding up to a total of about 1.5 mm from the beginning of  
14 the experiment (Table 1 cycle 13, and Figure 6), was measured returning from the second  
15 highest cycle at  $190^\circ\text{C}$  back to  $40^\circ\text{C}$ . Considering the effective blade bending  $l = \frac{g}{\omega^2} =$

16 336 mm of the GAS filter used, this drop corresponds to a 0.44% increase of the initial  
17 blade bending or an equivalent 0.44% loss of lifting power at constant position.

18 In other words, the measured fractional loss of lifting power at constant position is  
19 proportional to the load, but not proportional to the frequency of the filter. A 0.44%  
20 increase of the initial blade bending can be expected from any Maraging cantilever blade  
21 subject to the same stress level, with most of the effect showing up within the first year of  
22 service. As previously discussed, baking the filter under load corresponds to leaving the  
23 spring under load for an extended period of time. If we consider the exponential stretch of

1 time induced by higher temperatures, and that the creep is expected to be a logarithm of  
2 time, the data can be best summarized in the log-time plot of Figure 6. The linear fit in  
3 Figure 6 is in excellent agreement, over many orders of magnitude, with the expected  
4 logarithmic character of creep. With the assumed time expansion of a factor of 5 every  
5 10°C, the integrated effective experiment duration is equivalent to suspending the  
6 payload for  $10^{12}$  years (the time scale would be almost a million times longer if we had  
7 used the most probable creep acceleration factor of Table 1).

8

9 Table 1: Measured creep data. The time expansion factor is obtained using creep  
10 acceleration rate of  $1.174/^{\circ}\text{C}$  (corresponding to an assumed factor of 5 per  $10^{\circ}\text{C}$   
11 temperature increase). The effective ageing time (column 7) is obtained multiplying  
12 column 4 by column 6.

13

14 Figure 6: Integrated creep as a function of integrated effective ageing time. Only the  
15 measurements up to  $190^{\circ}\text{C}$  of table 1 are used in this plot because of the different  
16 observed creep at  $200^{\circ}\text{C}$ . The dot size corresponds to a measurement error of 30  
17 microns.

18

19 Figure 7: Linear creep rate observed when raising the oven temperature to  $200^{\circ}\text{C}$ .

20 The fit is compatible with a linear slope of  $18\pm 1$  mm/day.

21

22 The oven maximum temperature was  $200^{\circ}\text{C}$ . When the temperature was raised from  
23  $190^{\circ}\text{C}$  to  $200^{\circ}\text{C}$  an onset of linear creep behavior was detected (Figure 7) in sharp

1 contrast with the logarithmic behavior seen at lower temperatures. This very sharp  
2 threshold for the linear creep is an expected behavior in Maraging because its  
3 precipitates, which are all very similar to each other, do not interrupt the iron martensitic  
4 structure. The transition happens when there is sufficient stress in the material to allow  
5 dislocations to jump over the precipitates. As soon as the critical stress is reached, all  
6 dislocations can jump over all precipitates and move freely across the entire grain. The  
7 material is expected to switch from very elastic to very plastic. The sudden observed  
8 threshold is therefore an indication of the very good and uniform characteristics of the  
9 Maraging steel used.

10 The very limited slippage imposed on our sample is not expected to spoil the  
11 characteristics and behavior of the material.<sup>3</sup>

12 To cross check that the bake-out process has indeed burned out the creep, we then  
13 returned at 40°C and performed a long (120 day) stability measurement (Figure 8).

14 Linear fits to the data are compatible with zero slope, i.e. no detectable creep.

15 All of the above measurements were performed on blades bent to a 0.0047 surface strain,  
16 corresponding to a conservative 680 MPa stress (using Maraging's 145 GPa Young's  
17 modulus).

18

19 Figure 8: Long term stability check. The two curves show the same data histogrammed  
20 as raw data (left) and after applying to the data our best correction for the Young's  
21 modulus thermal change and for other external variables. The corrections are obtained

---

<sup>3</sup> Of course any real-life creep relieving procedure would be designed to maintain the metal well below the plastic transition and thus avoid any danger of plastic slippage.

1 using the information of auxiliary thermometers, and do not change the substance of the  
2 results.

3 The fits in the two curves,  $-0.11 \pm 0.1$  mm/day for the raw data and  $0.15 \pm 0.1$  mm/day  
4 for the corrected data are both compatible, within our measurement errors, with no creep.  
5 The opposite sign of the two slopes indicated that the measurement is dominated by  
6 systematics.

7

#### 8 **4. Creep Tests At Higher Strain**

9

10 A separate creep test, performed at various stress levels, including much higher stress,  
11 was performed in 2000. A number of triangular Maraging blades of different size and  
12 thickness were used in that earlier experiment. The bases of the blades were fastened at  
13  $45^\circ$  on the sides of a stand. Masses were loaded at the tip of each blade to bend it parallel  
14 to the floor. The triangular shape of these unconstrained blades insures constant  
15 curvature, and hence constant stress. The sizing of the individual blades was chosen to  
16 get the progression of stresses listed in Table 2, column 2. The thermal environment was  
17 a room-size, forced circulation enclosure where the temperature could be set at any  
18 temperature up to  $100^\circ\text{C}$  with a precision of  $0.020^\circ\text{C}/\text{week}$ . The forced air circulation  
19 was also inducing rapid thermalization of the blades. The droop of the blade tips was  
20 measured with LVDT position sensors, continually read-out at several kHz, and the  
21 averaged droop measurements were saved at 40 s intervals. This averaging washed out  
22 the random oscillation of the blades around their equilibrium position induced by the

1 forced air circulation. The experiment involved baking cycles as high as 80°C, each with  
2 typical durations of 2 weeks.

3 This was a much more complex experiment, and potentially more sensitive than the one  
4 described in Section 2 [13]

5

6 Figure 9: Example of creep (Arbitrary Units) at 30°C (<day 20), 40°C (21<day<37) and  
7 45°C (day>37). The line width of the logarithmic fit performed over the period between  
8 day 21 and day 36 completely covers the data points.

9

10 The experiment partially failed due to data acquisition failure (an automatic recalibration  
11 of the Data Acquisition 0 V baseline, happening at random times, corrupted data of long  
12 time baseline measurements at low creep speed), one example of which is visible in  
13 Figure 10. This failure is the reason we avoided using electronics readouts in the GAS  
14 spring tests of Section 2. The creep data was also polluted by the shrinking of the nylon  
15 LVDT coil supports as it lost its water content during the baking and possibly by small  
16 earthquake triggered changes of verticality of the pillar supporting the blades and by  
17 material hysteresis. Most of the data was eventually discarded because of these factors.  
18 The experiment was slated for repeat with new data acquisition cards from different  
19 manufacturers, peek LVDT supports, new blades, and stiffer footing, but was never run  
20 for lack of manpower.

21 In July 2007, that experiment was dismantled and the blades unloaded and measured.

22 The post mortem measurement data is reported in Table 2. Some blades were found to  
23 present a rather uniform permanent bend (blades 3, 4 and 9), indicating that they

1 underwent large creep. The blades that underwent sizeable creep were found to have a  
2 low Rockwell hardness, indicating faulty precipitation process or poor material. Since  
3 the precipitation process was performed at the same time on all 8 blades, and all the  
4 faulty blades have the same thickness and come from the same stock, we concluded that  
5 that sheet was either not well factory solubilized prior to our precipitation process (100  
6 hours at 435°C), or it was a mislabeled, different material.  
7 Significantly, the most stressed (1.5 GPa) blades showed no sign of permanent bend  
8 (within the original blade flatness), indicating that no significant creep had happened over  
9 the several weeks at different temperatures, including 2 weeks at 80°C and the 7 years at  
10 room temperature, a result in accord with the rest of the collected data.

11

12 Table 2: Blades recovered from Totem experiment.

13

14 These measurements show that well precipitated Maraging steel can withstand much  
15 more aggressive stress than what was applied in the cantilever blades used in HAM SAS,  
16 TAMA SAS, Advanced LIGO multiple pendula, and other systems. The measurements  
17 measured no anomalous creep up to 1.5 GPa, and up to 80°C. This stress level is quite  
18 close to the limit stress of 1.8 GPa measured at room temperature by Feng Gutong et al.  
19 [14] with Maraging wires hardened with this same precipitation process.

20 The observed failure of blades 3, 4 and 9 illustrate the importance of performing  
21 Rockwell Hardness tests on all Maraging blades before implementation, to ensure that the  
22 material has reached its design characteristics.

23

1 **5. Evaluation of the Arrhenius thermal creep rate acceleration.**

2  
3 The difficulty of estimating the Arrhenius thermal creep rate acceleration is to  
4 distinguish, during temperature transients, the relatively small variation of creep speed  
5 against the background of the much larger effects induced by the thermal variations of  
6 Young's modulus. We used some of the first experiment data when the creep was still  
7 fast and data corruption was not yet very significant and still under control. The final  
8 evaluation is the fruit of a long and progressive reduction of the error fork using several  
9 arguments.

10 Initially, we compared the creep speed change around the first temperature transient data  
11 (between 30°C and 40°C) of the six blades available at that time.

12 We used the creep plot themselves to evaluate the thermal transient time. We determined  
13 that the thermal transient started at hour 98.4, and that the blade had reached thermal  
14 equilibrium by hour 120. We also applied linear fits to the data segments before the  
15 transient and after hour 120. The ratios of the slopes before and after the transient (Figure  
16 10) were used as the measurement of the ratio of the actual creep speeds at the two  
17 temperatures. By ignoring the 20 hours during the temperature switch, we forfeited  
18 measurement of the initial phases thus underestimating the second slope and possible  
19 detection of any fast creep component that may be generated at the beginning of the  
20 thermal transient.

21  
22 Figure 10. Creep slope evaluation for a blade, before and after a 10°C temperature raise.

23 The linear fit before hour 98.4 and after hour 120 gave slopes of 0.00026 and 0.0016



1 respectively. The slope ratio of 6.11, from the fits in this figure, is the highest measured  
2 over the 6 blade measurements available. One of the DAQ jumps that eventually  
3 corrupted the long-term measurement is visible at about hour 115.

4

5 An average over the slope ratios of the fits performed on the available blades (slope  
6 ratios: 5.11, 4.95, 5.3, 6.11, 4.8, 5.16, 3.7) gave a mean of  $5 \pm 0.3$ , corresponding to a  
7 creep speed acceleration of  $1.175/^\circ\text{C}$ . This statistically seemed to promise a good quality  
8 measurement. The problem is that by waiting out the transient, the second slope is under-  
9 evaluated. In theory, this under-evaluation can be corrected by fitting the data with a  
10 logarithm function, and back extrapolating the slope to the moment just after the thermal  
11 transient.

12 To attempt to determine this time, exponential fits to the data accounting for the  
13 thermalization in addition to a logarithmic function for the creep were performed. The  
14 fits, one of which is shown in Figure 11, were of good quality. We found exponential  
15 thermalization constants of roughly 1.5 hours, reasonably consistent between all blades  
16 and with the air thermalization times in the enclosure. The exponentially fitted  
17 component of the droop was then subtracted from the data. The critical question was to  
18 (arbitrarily) decide how many thermalization time constants to wait for before picking the  
19 slope from the logarithmic fitted component of the data. The thermalization times, despite  
20 the forced air circulation, are still too large for a meaningful determination of the  
21 correction factor.

22 This indetermination yielded a correction factor of the order of 4, varying by a factor of  
23 2, which is clearly an unsatisfactory result.

1

2 Figure 11: Exponential and logarithmic fit to a thermal transient data set.

3

4 Having failed to effectively use the data of an up-step of temperature, we modified the  
5 original data gathering strategy, generated a temperature down-step and analyzed its data.

6 In a logarithmic function, the second derivative is  $1/t^2$ , drops faster than the slope itself  
7 ( $1/t$ ). In a temperature down-step, the error in extrapolation and the determination of the  
8 slope after the transient should be depressed.

9 This measurement was performed at 45°C, lowering the temperature to 40°C. A small  
10 (5°C) temperature step was chosen to obtain a still measurable slope at the lower  
11 temperature. From an average over several blades, we obtained a creep speed variation  
12 of

$$\frac{\sigma_{40^{\circ}C}}{\sigma_{45^{\circ}C}} = 0.202 \pm 0.025$$

13

14 In this analysis we realized that we had run into a different, but even more serious  
15 problem.

16 For about 7 to 8 days after the temperature drop (well beyond the several hours time scale  
17 of the Young's modulus variation effects) the creep data streams of all blades showed flat  
18 or negative curvature instead of the positive curvature expected from a logarithmic  
19 behavior. Only in the second week did the creep resume its normal logarithmic  
20 characteristic.

21

22 Figure 12

23

1 Figure 12 zoomed

2

3 Figure 12: Transient from 50°C to 45°C and up to 60°C and zoom on the 45°C region.

4 For a week after the temperature change, the creep graph curvature was inverted. This

5 effect, common to all blades, is better visible on the zoomed image, in which the vertical

6 scales of several blades have been shifted to illustrate the common behavior. Thermal

7 variation of the Young's modulus does not explain this effect, which supposedly may be

8 due to material hysteresis. Note that the temperature shown in the graph is shifted by 2°C

9 with respect to the temperature of the PID controller, reported in the text. This difference

10 between the two thermometers was stable to a few m°C level and has no effect in any of

11 the measurements reported.

12

13 We attributed this anomalous behavior to hysteresis in the blades (the effects of

14 hysteresis were eliminated in the GAS filter experiment of Section 2 by the excitation of

15 the vertical oscillation of the blades as discussed in reference [15]).

16 We therefore fell back on a third method.

17 We considered the end slope at the end of each of the following four baking period in the

18 30°C to 40°C and in the 50°C to 45°C. We chose these periods because they have the

19 same time length. The end slopes are supposedly far from either Young's modulus and

20 hysteresis transient perturbations. In the 30°C to 40°C temperature change, the initial

21 slope of the 40°C period is clearly underestimated, while in the 50°C to 45°C temperature

22 change, the initial slope of the 45°C period is clearly overestimated.

1 We can therefore safely use these two data sets to generate a lower and a higher limit of  
2 the thermal creep speed acceleration.

3

4 Table 3: Evaluation of upper and lower limit of the Arrhenius thermal creep speed  
5 acceleration.

6

7 From this data we determined an Arrhenius acceleration of  $1.28 \pm 0.13 / ^\circ\text{C}$ .

8

9 From the measured Arrhenius acceleration of the drift speed change one can estimate the  
10 activation energy  $E_{act}$  of the dislocations responsible for creep. Maraging (and all  
11 crystalline metals in general) have a very large pool of dislocations. Some, uninteresting,  
12 are completely pinned down, some are sitting against precipitates and stick to them with  
13 various binding energies, depending on the type of dislocation and precipitates. Of these,  
14 the ones with activation energies below or near thermal energies ( $kT$ ) are completely free  
15 to move, and can contribute to hysteresis. The dislocations that induce creep are the  
16 unstable ones with binding energies much above  $kT$  (of course only the dislocations  
17 sitting against precipitates on the downslope of the stress field can gain energy in moving  
18 and are unstable.). These can be activated only by large local fluctuations of thermal  
19 energy. The probability that a thermal fluctuation is large enough to reach up to  $E_{act}$  can  
20 be written as  $e^{-\frac{E_{act}}{kT}}$ . The creep speed  $\sigma$  can then be written as the product of a slowly  
21 varying constant  $\alpha(t)$  (proportional to the number of the remaining available dislocations,  
22 which are slowly used up in the creep process;  $\alpha(t)$  has logarithmic behavior to reflect

1 the progressive depletion of the available dislocation pool) times the mean dislocation  
 2 thermal activation probability. The creep speed has then the form  $\sigma = \alpha(t) \cdot e^{-\frac{E_{act}}{KT}}$ .  
 3 Using the creep speed measurements before and after a sudden temperature change, we  
 4 obtain:

$$\begin{aligned} 5 \quad \sigma_1 &= \alpha(t) \cdot e^{-\frac{E_{act}}{kT_1}} \\ 6 \quad \sigma_2 &= \alpha(t) \cdot e^{-\frac{E_{act}}{kT_2}} \\ 7 \quad \ln \frac{\sigma_1}{\sigma_2} &= \frac{E_{act}}{kT_2} - \frac{E_{act}}{kT_1} = E_{act} \frac{T_1 - T_2}{kT_1 T_2} \\ 8 \quad E_{acr} &= \frac{kT_1 T_2}{T_1 - T_2} \ln \frac{\sigma_1}{\sigma_2} \\ 9 \quad E_{act-max} &= 0.86 \cdot 10^{-4} \cdot 303 \cdot 313 \cdot \ln(1.139) = 1.06 \text{eV} \\ 10 \quad E_{act-min} &= 0.86 \cdot 10^{-4} \cdot 318 \cdot 323 \cdot \ln(1.413) = 3.05 \text{eV} \\ 11 \quad E_{act} &= 2.0(\pm 1.0) \text{eV} \\ 12 \end{aligned}$$

## 13 6. Measurement of the thermal variation of the Young's modulus

14  
 15 The thermal variation of the Maraging Young's modulus was made in two ways.

16 In the first method the thermal change of the spring lifting power was measured from the  
 17 data of Table 1, column 3, when returning to a lower temperature level. This estimation  
 18 was not made on the up-transients to higher temperature levels to offset the effects of  
 19 creep.

20 Only the transients from 40 to 30°C, from 60 to 40°C and from 90 to 40°C were used  
 21 (Table 4) because for higher temperature steps changes in payload were required.

22 The thermal droop was transformed in lifting power change using a position versus load  
 23 data previously gathered at 30°C.

1

2 Table 4: Determination of the thermal change of the Young's modulus.

3

4 A weighted average of the three data points yielded a value of  $2.16(\pm 0.07) \times 10^{-4}/^{\circ}\text{C}$  for  
5 the thermal change of the Young's modulus.

6

7 An independent determination of the thermal change of the Young's modulus was  
8 performed with a virtually identical GAS filter during the course of a separate experiment  
9 [16]. This filter was equipped with a coaxial LVDT position sensor and a voice coil  
10 actuator. A feedback between the sensor and the actuator with a 1000 second time  
11 constant integration filter was used to maintain the vertical position of the filter at its  
12 working point while the ambient temperature changed between 22.5 and 23°C.

13 The voice coil current was monitored as a measurement of the correction force necessary  
14 to compensate for the change of Young's modulus. The voice coil force versus current  
15 slope was measured by adding known masses on the payload and noting the jumps in  
16 feedback current on the actuator. The data thus calibrated is shown in Figure 13. The fit  
17 gives a value of  $2.20 \times 10^{-4}/^{\circ}\text{C}$  for the thermal change of the Young's modulus with a  
18 0.25% statistical error on the fit, a 0.3% error in the payload determination, and a similar  
19 error in the voice coil calibration. Adding up in quadrature these three errors, we get a  
20 0.5% error on the measurement, i.e.  $2.217(\pm 0.011) \times 10^{-4}/^{\circ}\text{C}$ .

21 Combining the two measurements, which marginally agree within their errors, we obtain  
22  $2.203 (\pm 0.013) \times 10^{-4}/^{\circ}\text{C}$ .

23

1 Figure 13: Correction force necessary to maintain the GAS spring at its working point as  
2 temperature changes.

3

#### 4 **7. Conclusions**

5 We measured creep in stressed Maraging blade springs over extended periods of time and  
6 different temperatures. We observed a creep of 0.44% of the original blade bending.

7 Similar creep levels can be expected over the years in any system made with loaded  
8 Maraging blades. Simply baking the blades under their nominal stress can eliminate the  
9 creep effects.

10 We measured a thermal variation of the Young's modulus of  $2.023 (\pm 0.013) 10^{-4}/^{\circ}\text{C}$ .

11 We estimated an Arrhenius thermal variation of creep speed of  $1.28 \pm 0.13/^{\circ}\text{C}$  and a  
12 dislocation activation energy of  $E_{act} = 2.0 (\pm 1.0) \text{eV}$ .

13 Including the Arrhenius acceleration factor, we achieved spring ageing of 100 billion  
14 years. We verified that no residual creep is detectable after this heat treatment.

15 We found that blades stressed at 680 MPa presented normal logarithmic creep up to a  
16 temperature of  $190^{\circ}\text{C}$ , but experienced linear runoff creep at  $200^{\circ}\text{C}$ .

17 Well hardened blades, stressed up to 1.48 GPa, did not show any excess creep up to  
18 temperatures of  $80^{\circ}\text{C}$ .

19

#### 20 **Acknowledgements**

21

22 In memory of Michael Koyfman, he gave us a great example of friendship and courage.

23 We would like to thank the National Science Foundation which granted for the SURF

1 program, Caltech and the SURF office.  
2 The LIGO Observatories were constructed by the California Institute of Technology and  
3 Massachusetts Institute of Technology with funding from the National Science  
4 Foundation under cooperative agreement PHY 9210038. The LIGO Laboratory operates  
5 under cooperative agreement PHY- PHY-0107417. This paper has been assigned LIGO  
6 Document Number LIGO-P070095-00-Z.

## 8 **References**

- 9
- 10 [1] The creep problem in the VIRGO suspensions: a possible solution using Maraging  
11 steel., M. Beccaria, . . . , V. Rubino, et al., Nuclear Instruments & Methods in Physics  
12 Research, 1998, vol. 404, no 2-3, pp. 455-469
- 13 [2] Riccardo DeSalvo, “Non-stochastic noise in gravitational wave detectors”, second  
14 Edoardo Amaldi conference on Gravitational waves, CERN Switzerland, 1-4 July  
15 **1997** World Scientific Publishing Co, P.O. Box 128 Farrer Road, Singapore 912805,  
16 page 228-239, LIGO Document No. P970036-00-D, available at  
17 <http://admdbsrv.ligo.caltech.edu/dcc/>
- 18 [3] G. Cella “Monolithic geometric anti-spring blades” Nuclear Instruments and Methods  
19 in Physics, Volume 540, Issues 2-3, 21 March 2005, pp. 502-519
- 20 [4] A. Bertolini, et al., “Design and prototype tests of a Seismic Attenuation System for  
21 the Advanced-LIGO Output Mode Cleaner”, Class. Quantum Grav. 23 (2006) S111–  
22 S118 LIGO document LIGO-P050024-00-D, available at  
23 <http://admdbsrv.ligo.caltech.edu/dcc/>



- 1 [5] Alberto Stochino, Doctoral thesis, Dipartimento di Fisica “Enrico Fermi”, Università  
2 di Pisa, Largo Bruno Pontecorvo, I-56127 Pisa, July 2007, LIGO Document No.  
3 P070083, available at <http://admdbssrv.ligo.caltech.edu/dcc/>
- 4 [6] Beccaria, M., et al., 1997, “Extending the Virgo Gravitational Wave Detection  
5 Band Down to a few Hz, Metal Blade Springs and Magnetic Antisprings,”  
6 Nucl. Instrum. Methods Phys. Res. A, **394**, pp. 397–408
- 7 [7] R. DeSalvo, “Passive, non-linear, mechanical structures for Seismic Attenuation”,  
8 Journal of Computational and Non-Linear Dynamics”, Vol 2, pag 290-298, October  
9 2007. And references therein.
- 10 [8] A New Seismic Attenuation Filter Stage MGASF For Advanced Gravitational Wave  
11 Interferometric Detectors, V. Sannibale, A. Bertolini, G. Cella, R. DeSalvo, S Ma`rka, K.  
12 Numata}, A.Stochino, A Takamori, H. Tariq, to be Submitted to NIM-A
- 13 [9] Alberto Stochino, graduation thesis, Dipartimento di Fisica "Enrico Fermi" ,  
14 Università di Pisa, Largo Bruno Pontecorvo, I-56127 Pisa, Italy, Document no.  
15 P06004400-D, available at <http://admdbssrv.ligo.caltech.edu/dcc/>
- 16 [10] (ref. Maraging steel has been used in this super-plastic regime as a damping  
17 material to absorb the rocket vibration in the Apollo capsule seats, private  
18 communication, David Platus, Minus K Technology, 420 S. Hindry Ave., Unit E  
19 Inglewood, CA 90301, <http://www.minusk.com>)
- 20 [11] A. Takamori, “Low Frequency Seismic Isolation for Gravitational Wave Detectors”,  
21 Doctoral Thesis, University of Tokyo (2003) LIGO Document No. P030049, available at  
22 <http://admdbssrv.ligo.caltech.edu/dcc/>
- 23 [12] Nicole Virdone, et al., Preliminary results from the measurement of creep in

1 Maraging blades LIGO technical note Document no. T050047-00-R, available at  
2 <http://admdbsrv.ligo.caltech.edu/dcc/>  
3 [13] Rosalia Stellacci, Dipartimento di Fisica "Enrico Fermi" , Università di Pisa, Largo  
4 Bruno Pontecorvo, I-56127 Pisa, Italy, Document no. P020049-00-R , available at  
5 <http://admdbsrv.ligo.caltech.edu/dcc/P020049-00-R>  
6 [14] F. Gutong, S. Braccini, C. Casciano, V/ Dattilo, R. DeSalvo, F. Frasconi, G.  
7 Gennaro, R. Passaquieti, R. Valentini. CNRS, INFN, & VIRGO internal report. Ref:  
8 VIR-TRE-PIS-4600-129. June 1997  
9 [15] DeSalvo, R., et al., 2005, "Study of Quality Factor and Hysteresis Associated  
10 with the State-of-the-Art Passive Seismic Isolation System for Gravitational  
11 Wave Interferometric Detectors," Nucl. Instr. and Meth., Volume 538, Issues 1-3, 11  
12 February 2005, Pages 526-537.  
13 [16] Mantovani, M., and DeSalvo, R., 2004, "One Hertz Seismic Attenuation for Low  
14 Frequency Gravitational Waves Interferometers," Nucl. Instr. and Meth., Volume 554,  
15 Issues 1-3, 1 December 2005, pp. 546-554

1 **TABLES**

2 Table 1: Measured creep data. The time expansion factor is obtained using creep  
3 acceleration rate of  $1.174/^{\circ}\text{C}$  (corresponding to an assumed factor of 5 per  $10^{\circ}\text{C}$   
4 temperature increase). The effective ageing time (column 7) is obtained multiplying  
5 column 4 by column 6.

Cycle	Temperature [°C]	Creep Saturation level [mm]	Cycle Duration [days]	Measured creep [mm]	Time expansion (acceleration) factor	Effective ageing time in cycle [days]	Integrated effective ageing time [years]
1	30	9.28	1		3.6	3.62	9.93E-03
2	40	8.69	4	0.00	18	72.5	2.08E-01
3	30	9.17	2		3.6	7.25	2.28E-01
4	60	7.18	41	0.26	4.5E+02	1.86E+04	5.11E+01
5	40	8.43	8		18	145	5.15E+01
6	90	4.93	20	0.56	5.7E+04	1.13E+06	3.15E+03
7	40	8.13	20		18	362	3.16E+03
8	150	2.07	19	1.17	8.8E+08	1.68E+10	4.61E+07
9	40	7.52	7		18	127	4.61E+07
10	170	3.36	27	1.33	2.2E+10	5.97E+11	1.68E+09
11	40	7.36	7		18	127	1.68E+09
12	190	2.96	14	1.51	5.5E+11	7.74E+12	2.29E+10
13	40	7.18	10		18	181	2.29E+10
14	200	2.00	20	1.73	2.8E+12	5.53E+13	1.74E+11
15	40	6.96	118		18	2.14E+03	1.74E+11

1 Table 2: Blades recovered from Totem experiment.

Blade #	Stress [GPa]	Permanent bend [mm]	Rockwell A hardness	Blade thickness [mm]	Nom. Blade bending radius [mm]
1	0.735	1.5	51.8	2.97	293
2	0.735	0.50	52.0	2.97	293
3	0.824	10	30.1	3.33	293
4	0.829	7.0	30.4	3.35	293
5	0.948	0.50	52.3	3.83	293
6	0.960	0.50	51.9	3.88	293
7	1.124	1.0	52.5	2.96	191
8	1.127	1.0	52.2	2.97	191
9	1.272	21	34.0	3.35	191
10	unloaded	0	29.8	3.37	191
11	1.484	0.0	52.9	3.91	191
12	1.484	0.0	52.4	3.91	191

2

- 1 Table 3: Evaluation of upper and lower limit of the Arrhenius thermal creep speed
- 2 acceleration.

Drift speed thermal acceleration	Lower limit x/°C	Upper limit x/°C
Blade 1	1.1093	1.3747
Blade 2	1.1525	1.4171
Blade 3	1.1103	1.4424
Blade 4	1.1140	1.4945
Blade 5	(1.2342)	1.4310
Blade 6	1.1514	1.3356
Blade 7	1.0985	1.3488
Blade 8	1.1387	1.4572
Mean	1.139	1.413
Std Deviation	0.044	0.055

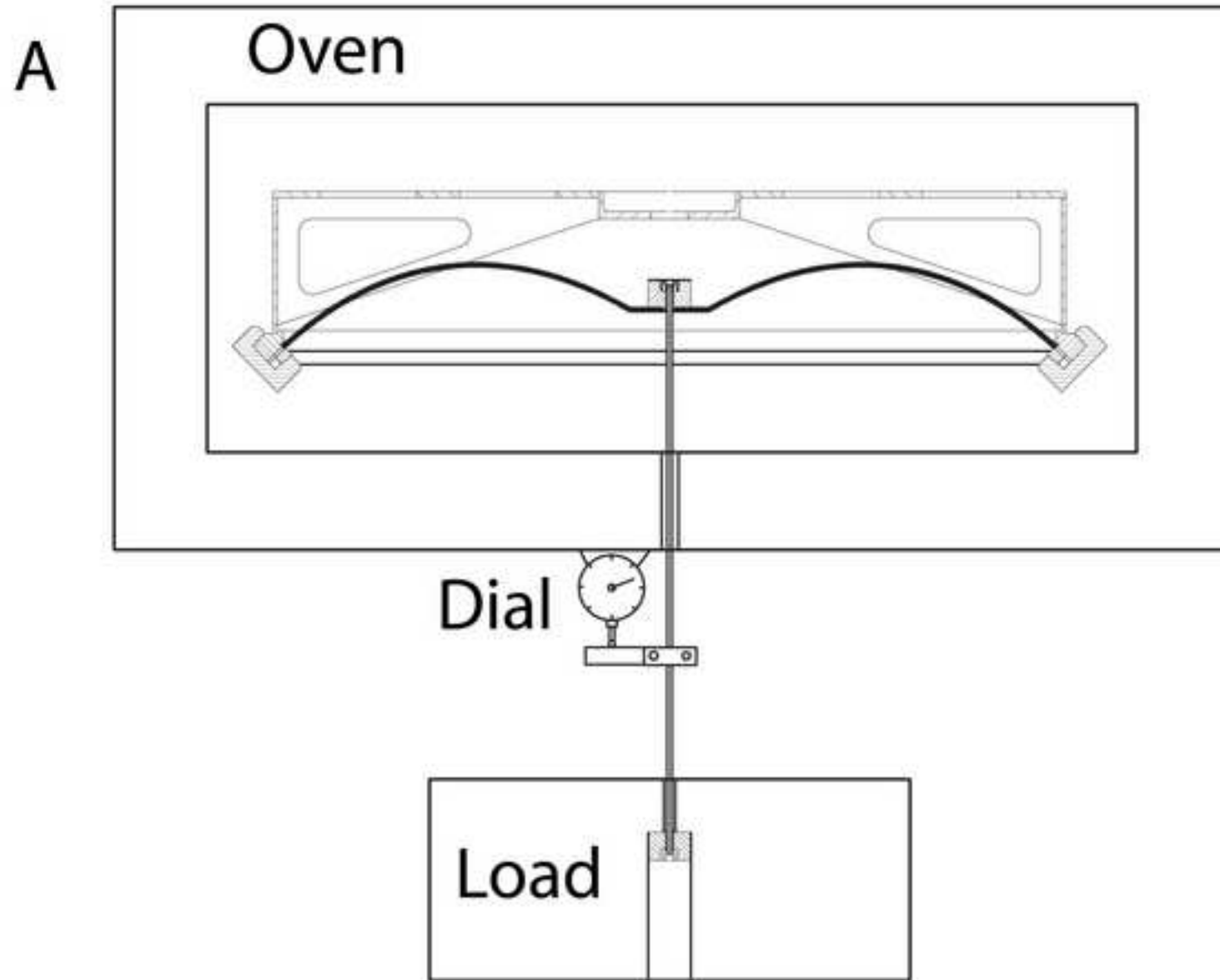
3

1 Table 4: Determination of the thermal change of the Young's modulus.

Initial T	End T	DT	Droop	Hoist power loss	Young's modulus variation	
°C	°C	°C	mm	gram	1/°C	
40	30	10	0.48	107.2	1.7	$\times 10^{-4}$
60	40	20	1.25	279.1	2.19	$\times 10^{-4}$
90	40	50	3.2	714.6	2.24	$\times 10^{-4}$

2

Figure 1a  
[Click here to download high resolution image](#)





**B**

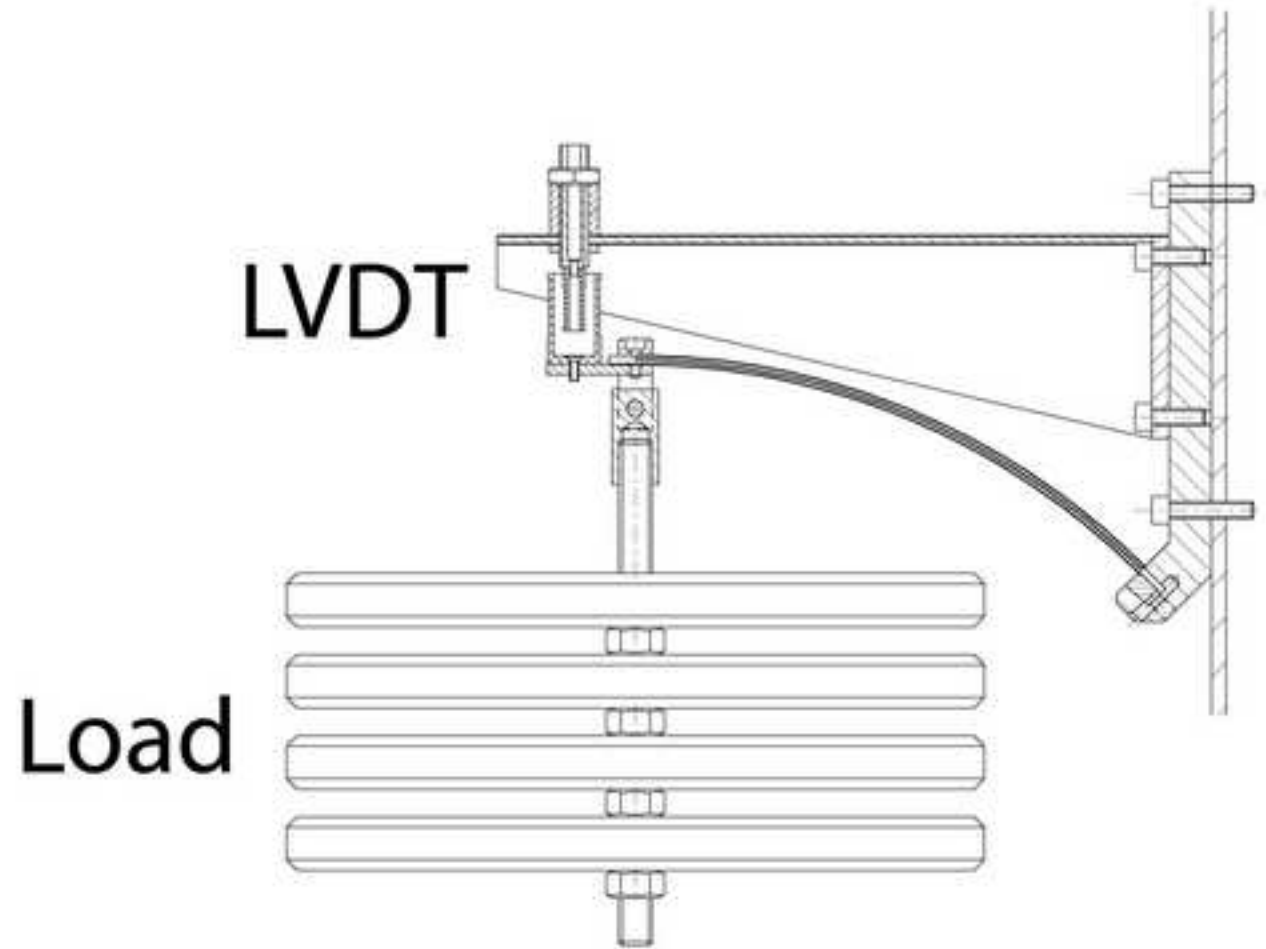


Figure 2  
[Click here to download high resolution image](#)

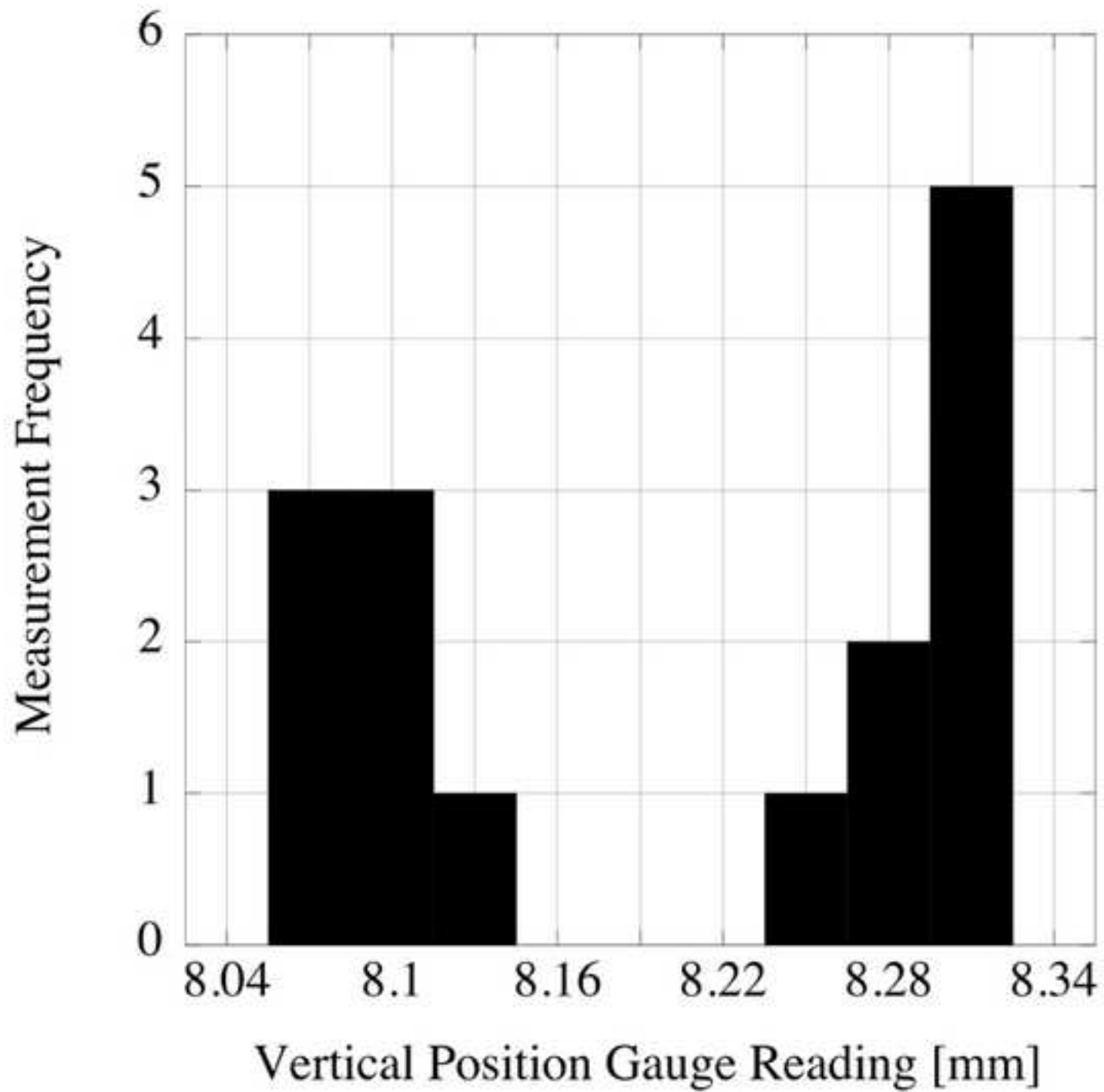


Figure 3  
[Click here to download high resolution image](#)

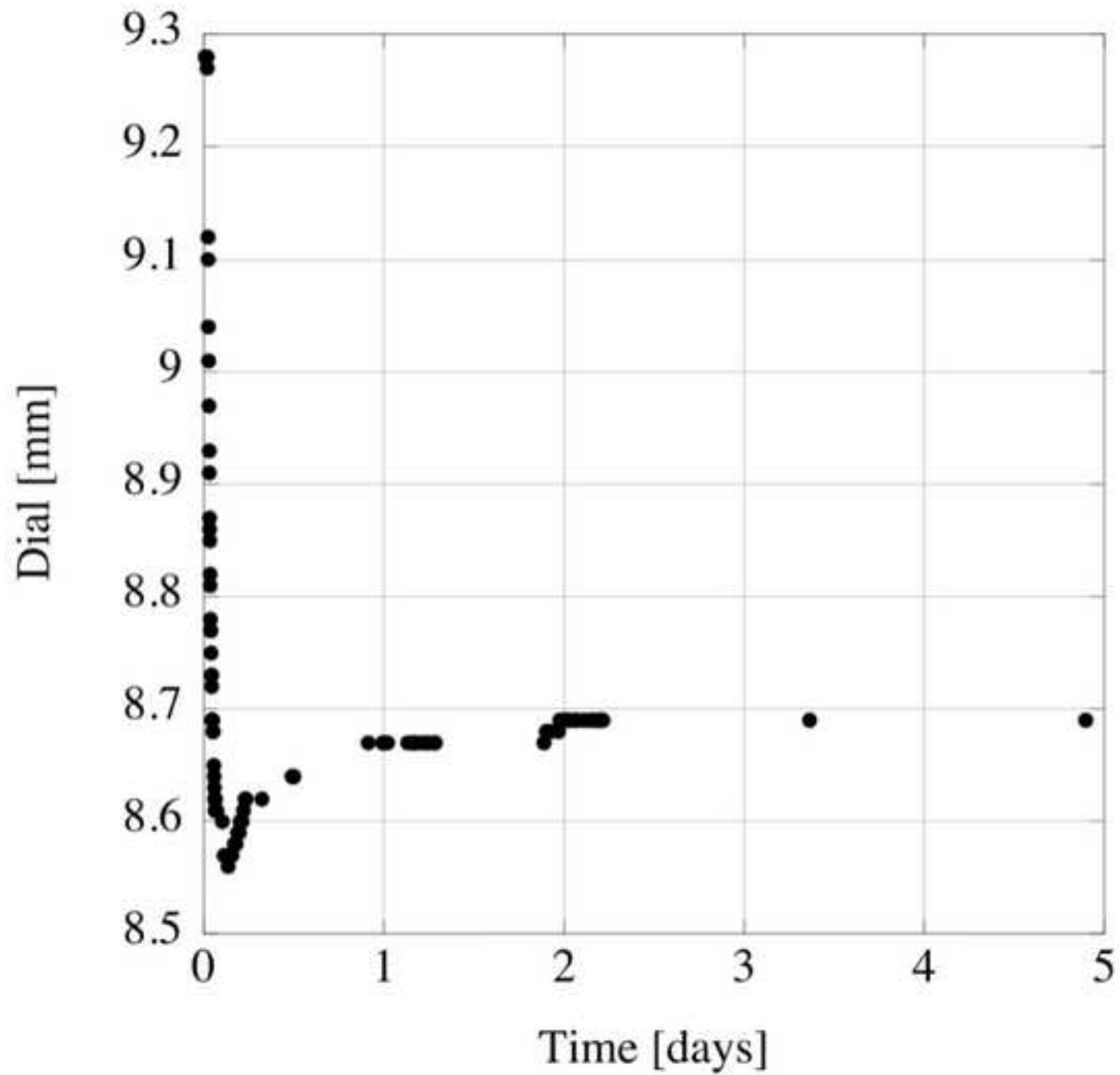


Figure 4  
[Click here to download high resolution image](#)

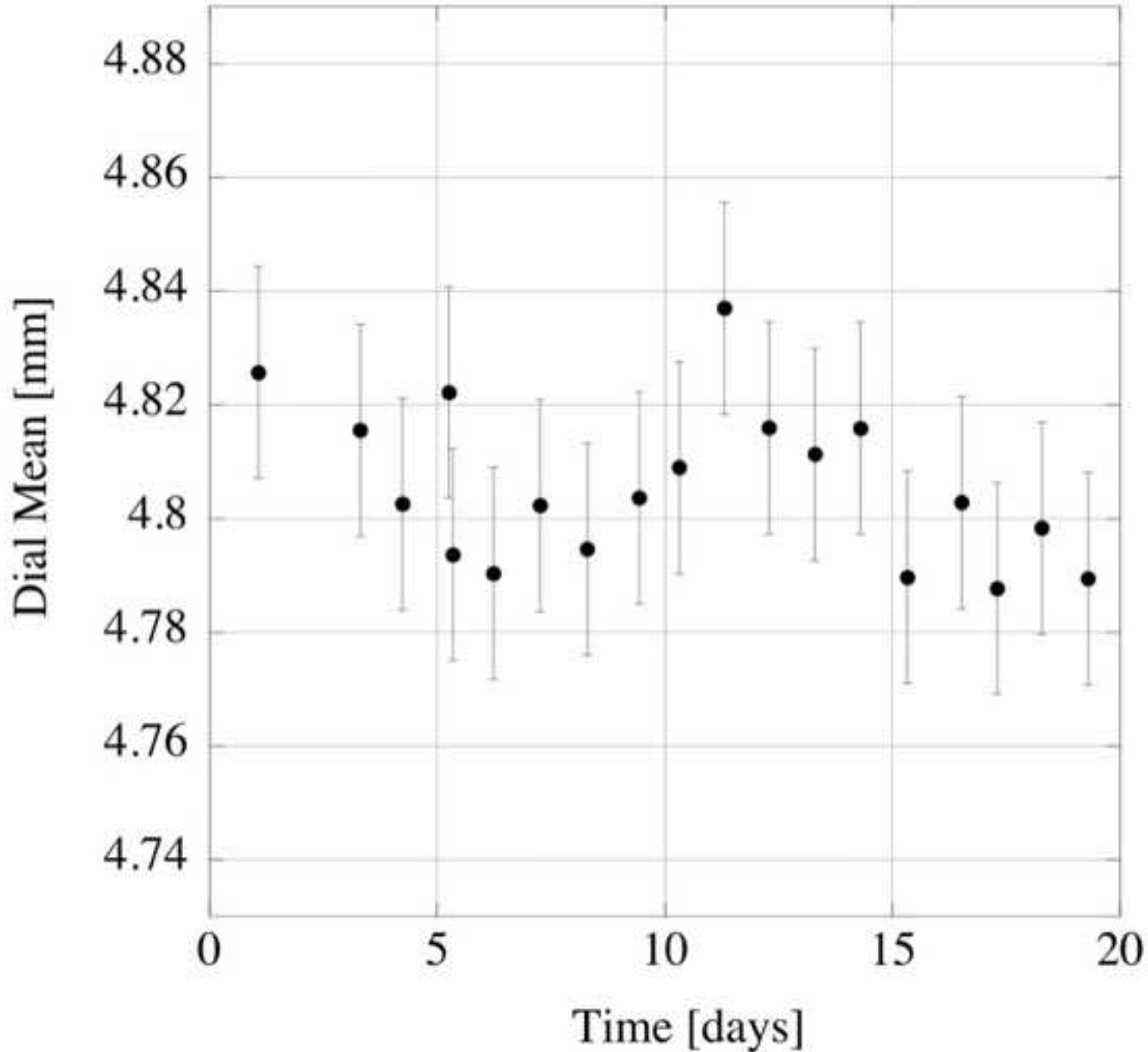


Figure 5a  
[Click here to download high resolution image](#)

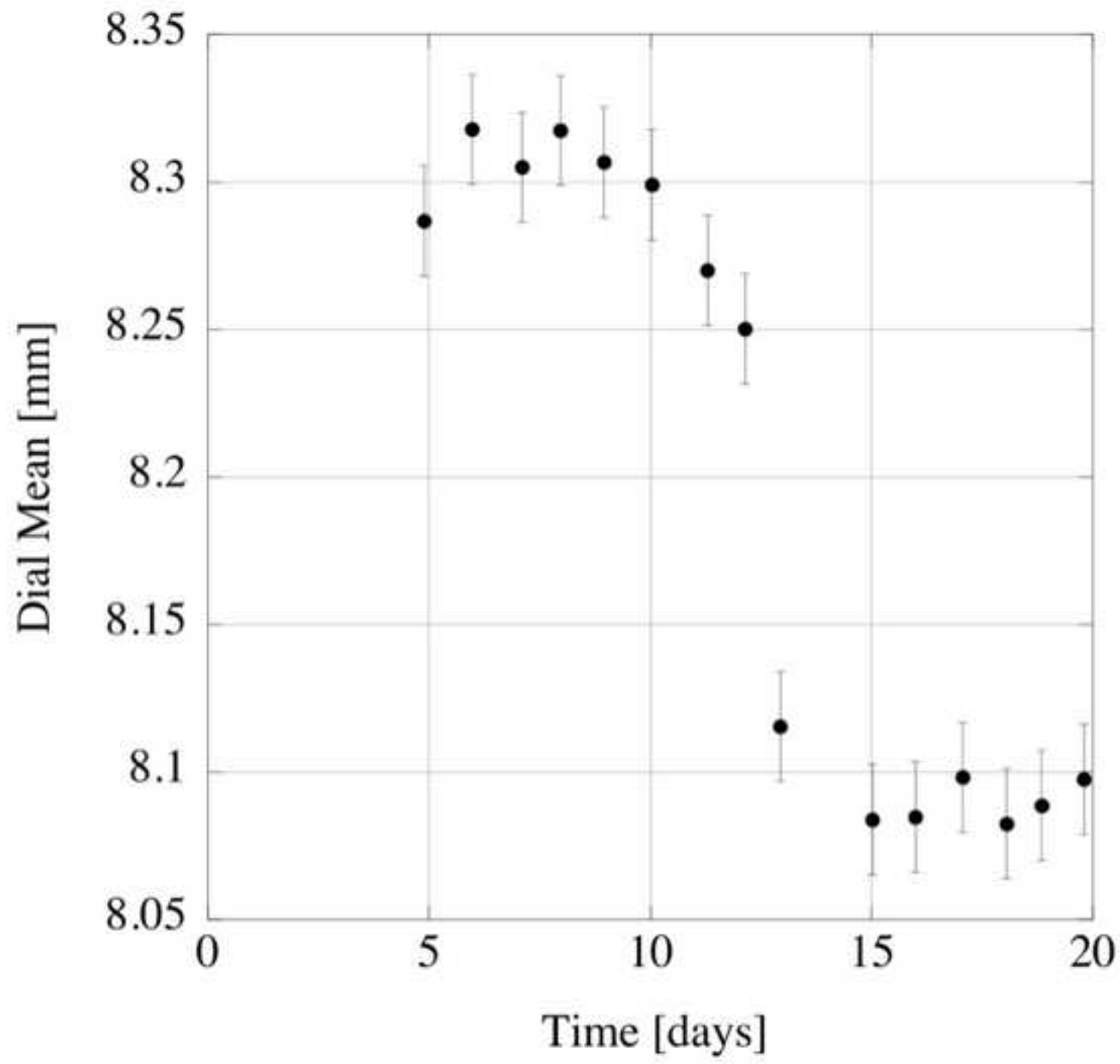


Figure 5b  
[Click here to download high resolution image](#)

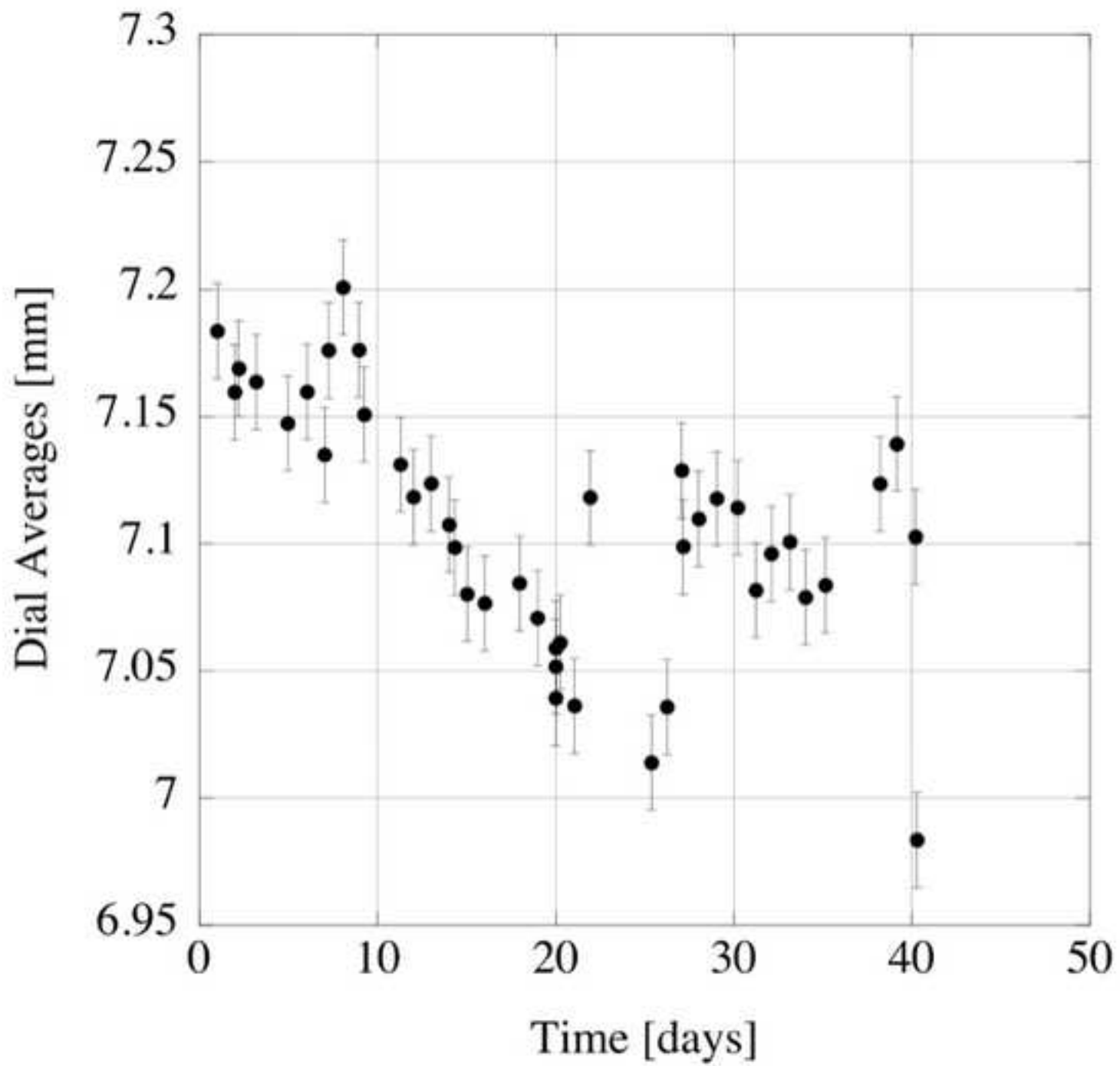


Figure 6  
[Click here to download high resolution image](#)

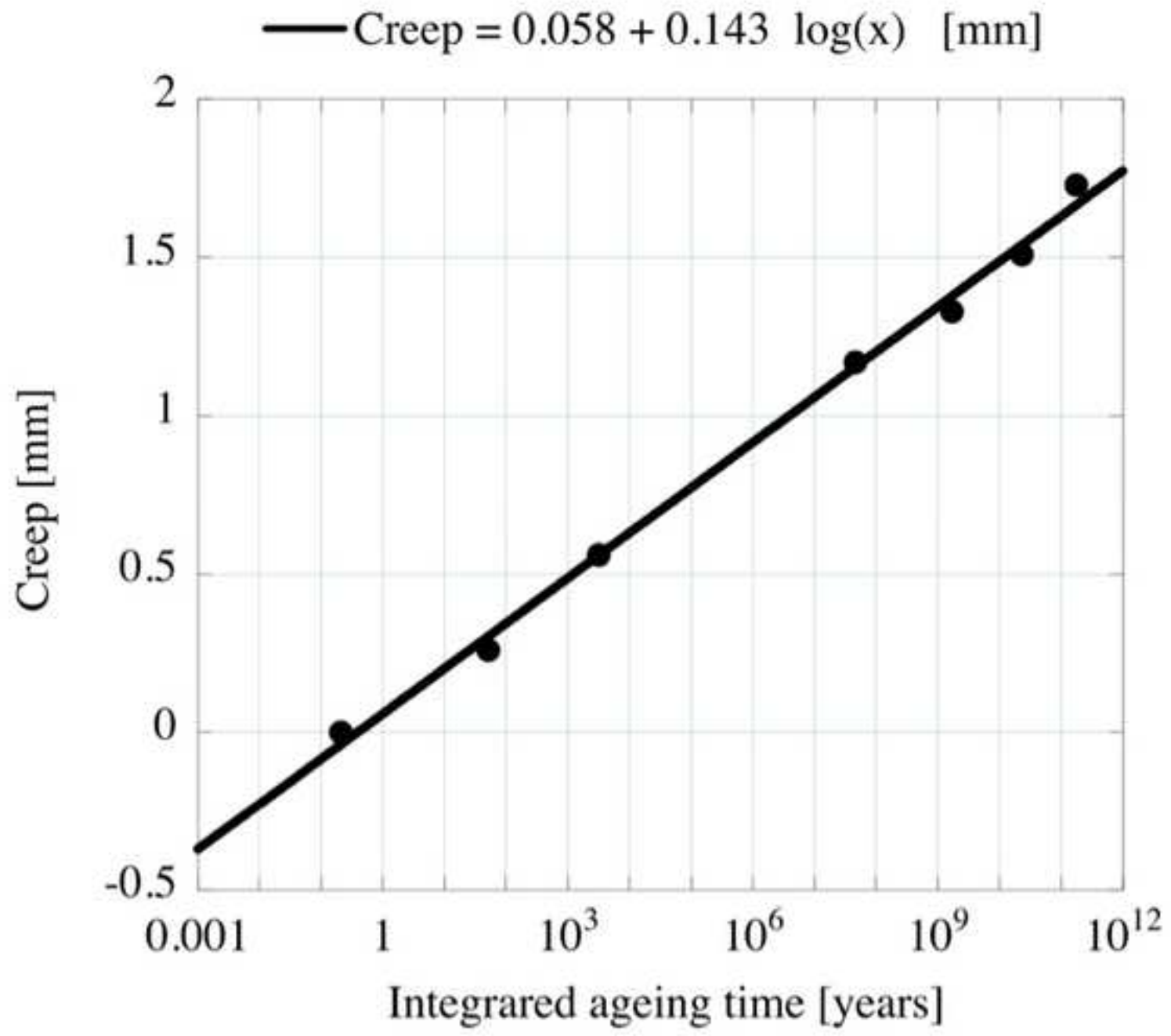


Figure 7  
[Click here to download high resolution image](#)

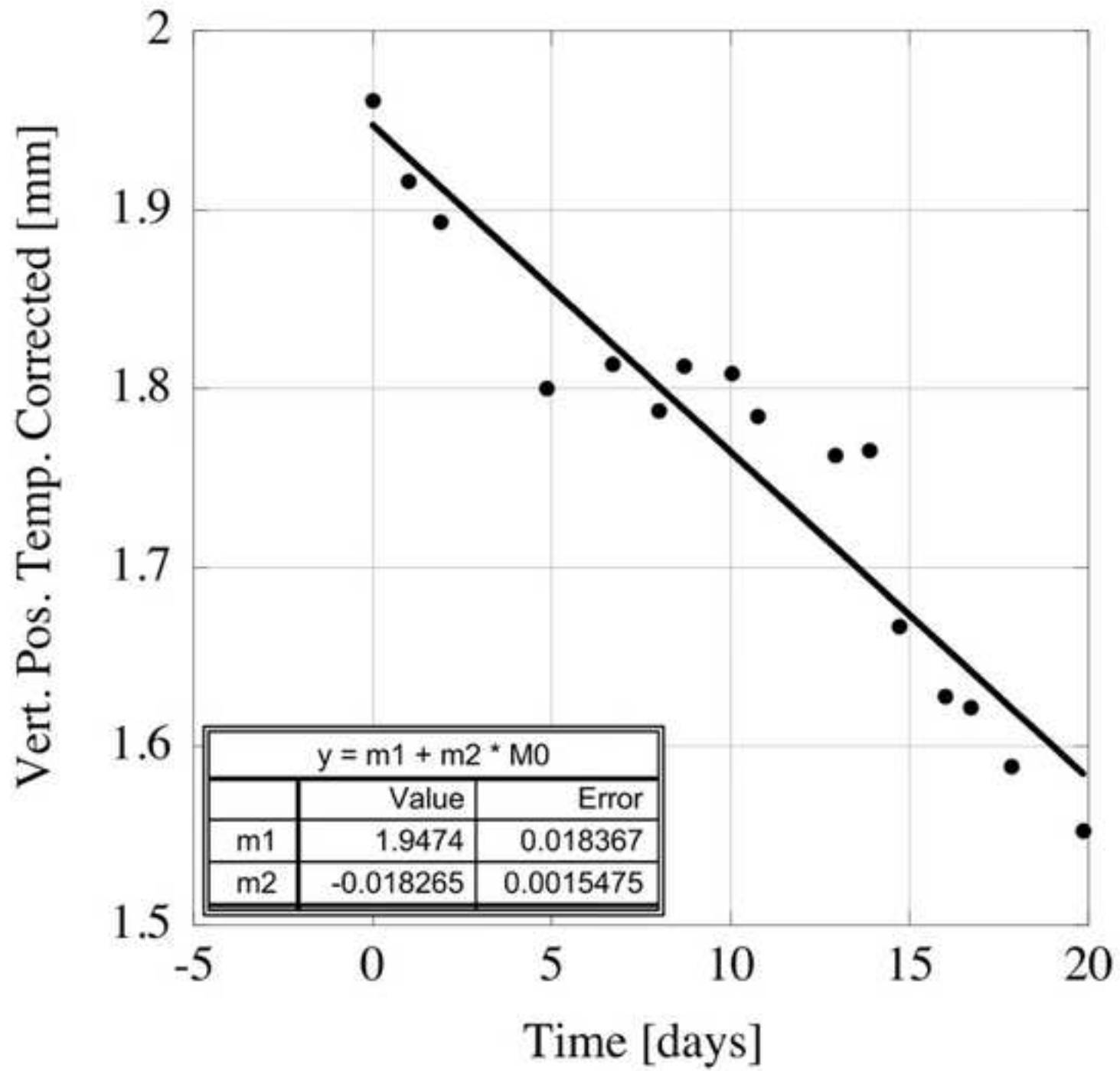




Figure 8a  
[Click here to download high resolution image](#)

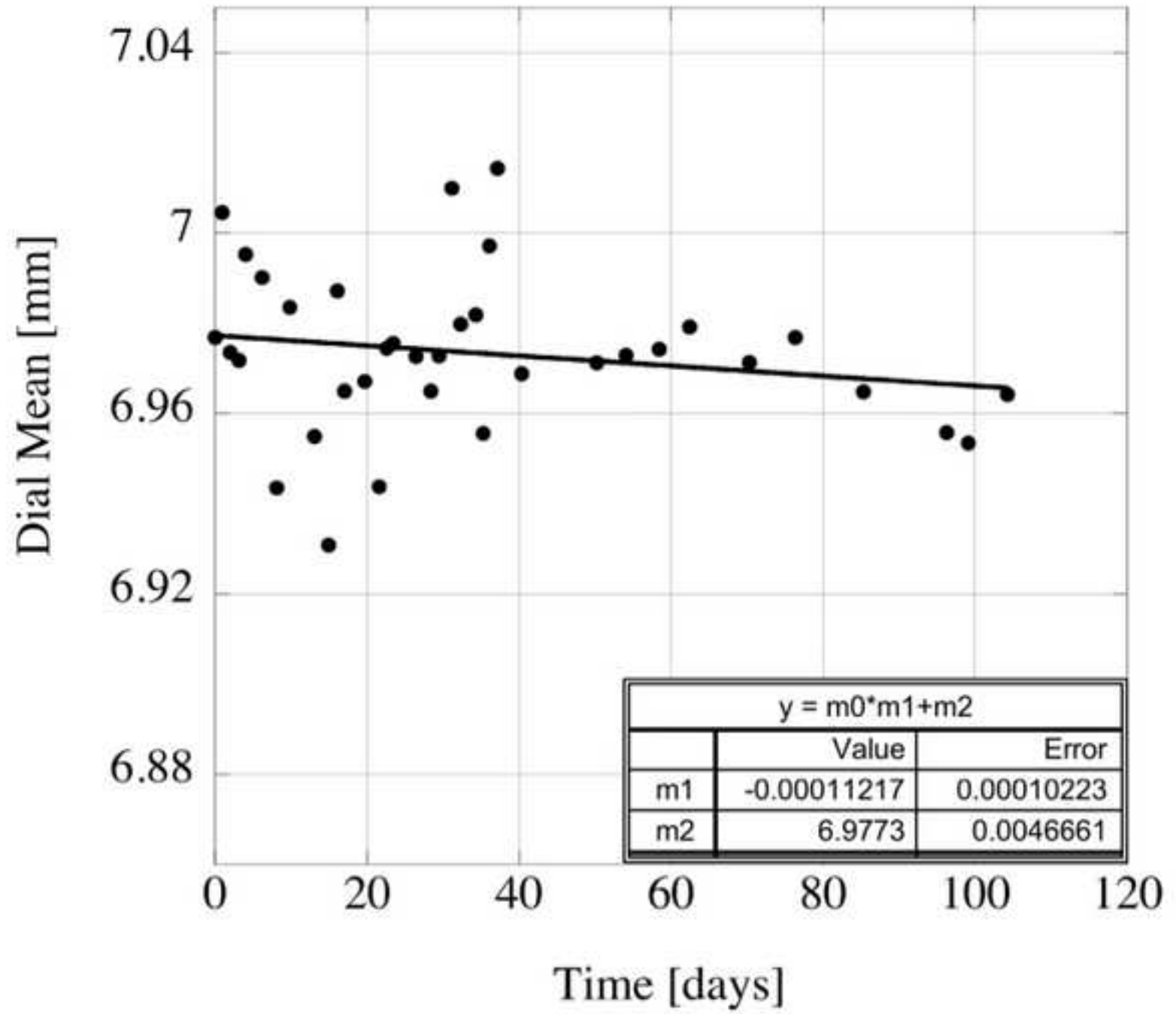


Figure 8b  
[Click here to download high resolution image](#)

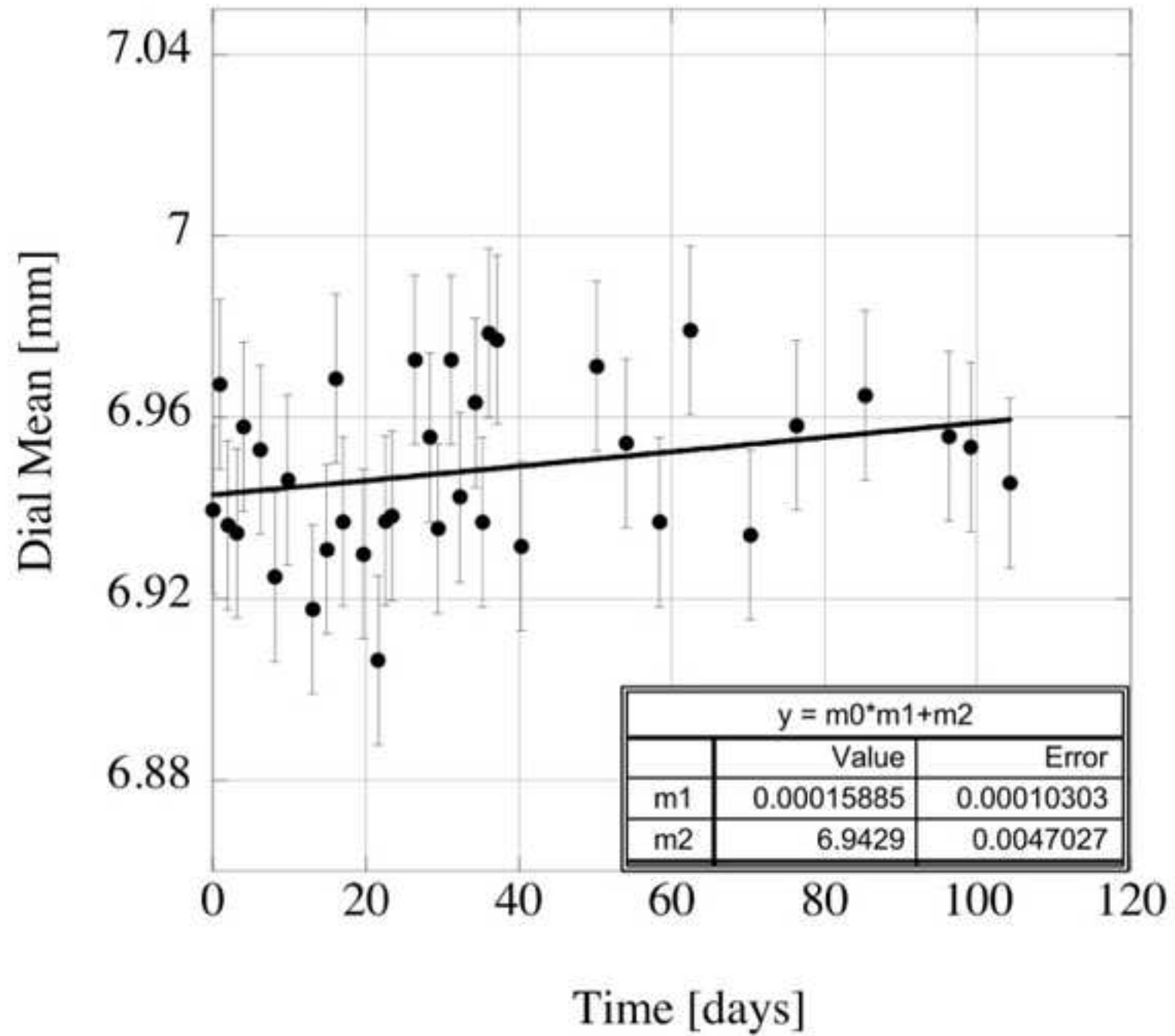


Figure 9  
[Click here to download high resolution image](#)

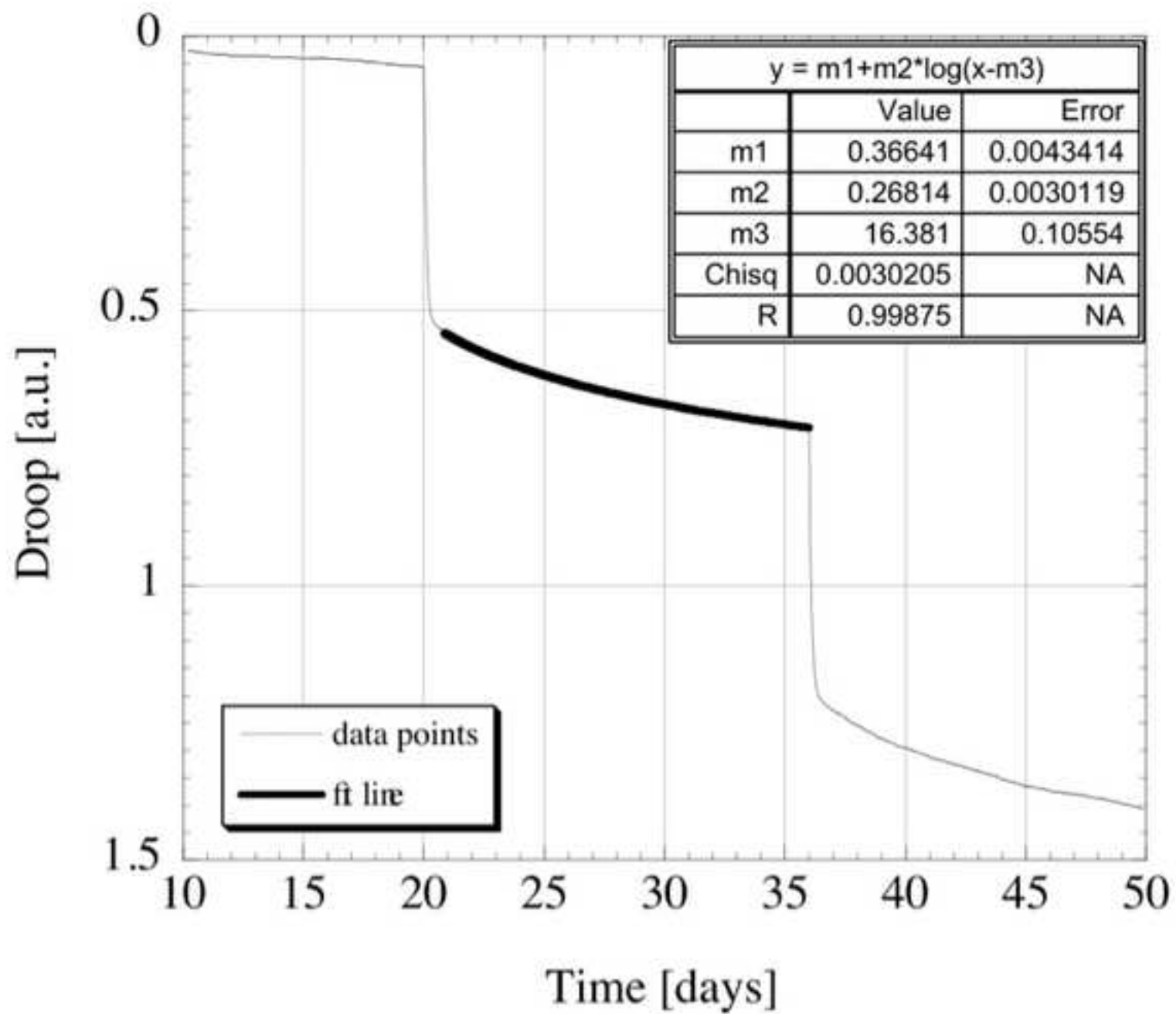


Figure 10  
[Click here to download high resolution image](#)

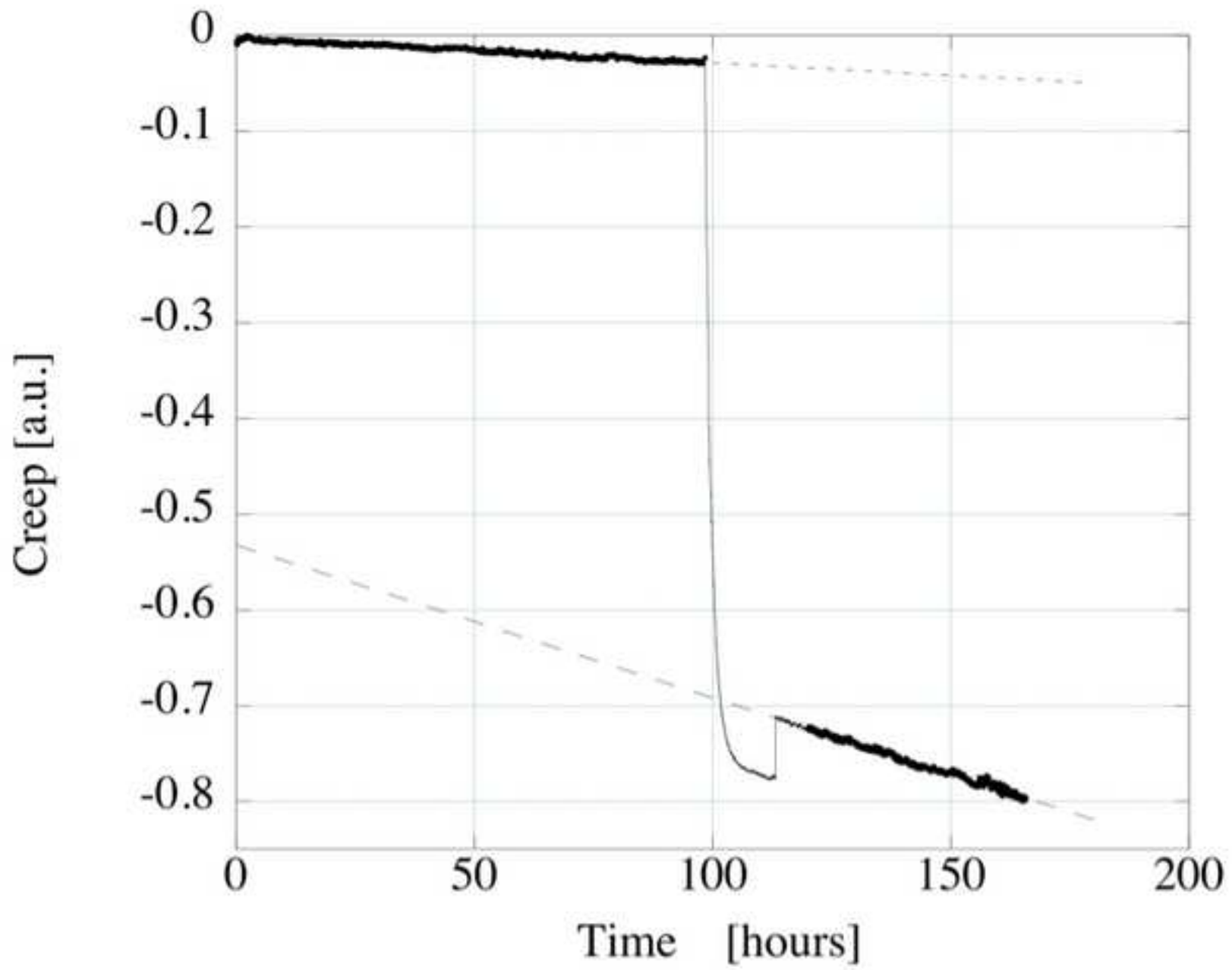


Figure 11

[Click here to download high resolution image](#)

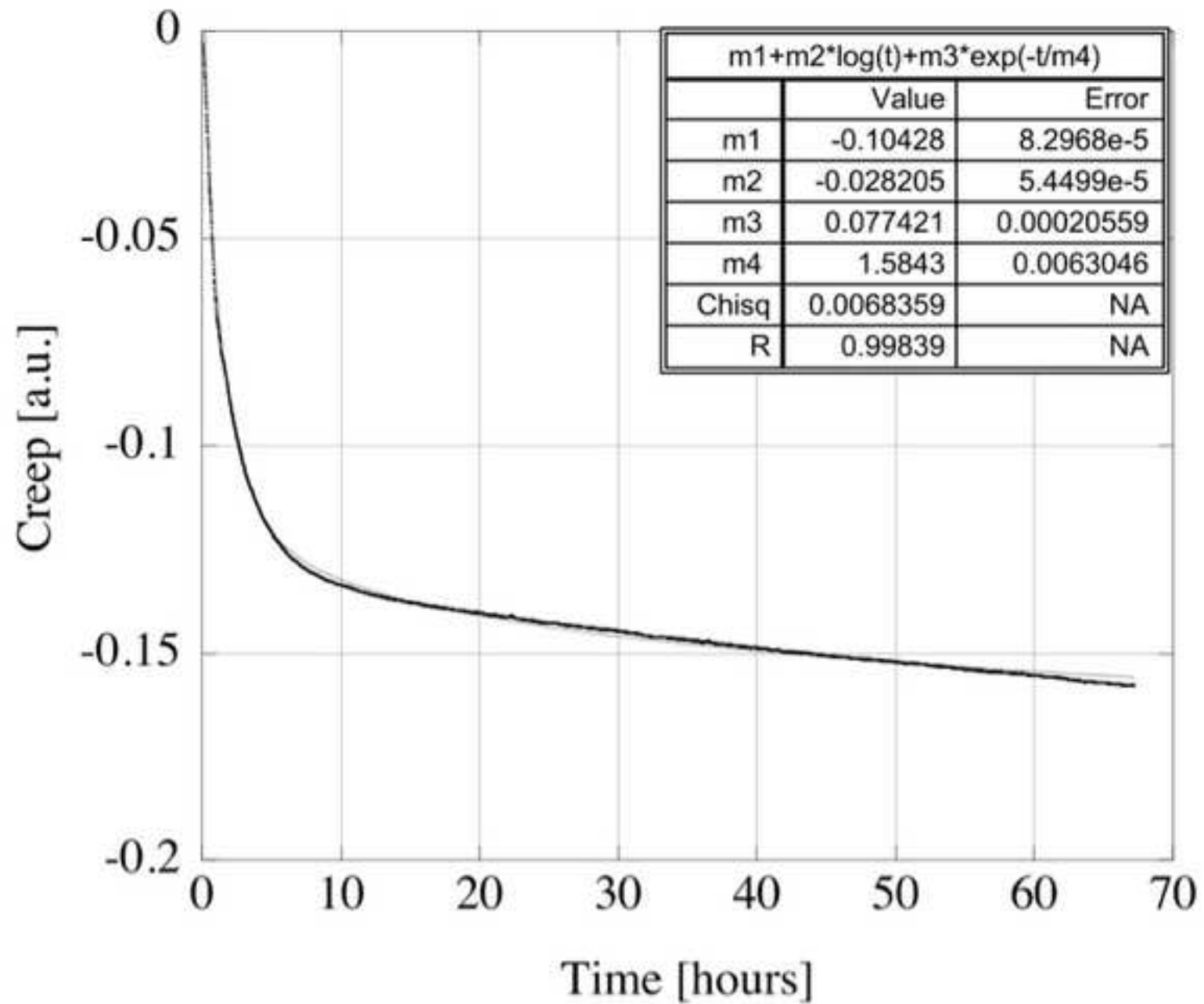


Figure 12a  
[Click here to download high resolution image](#)

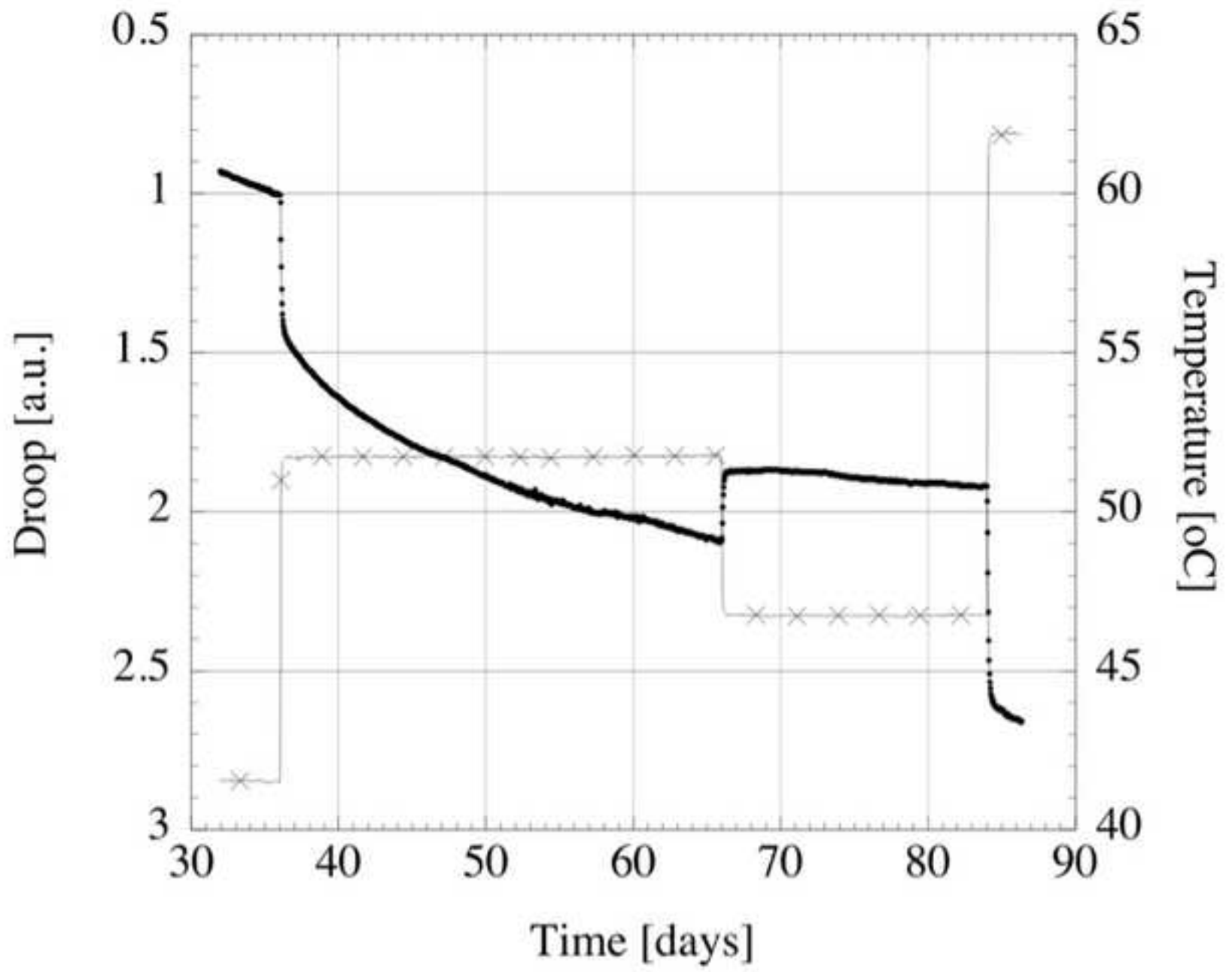


Figure 12b  
[Click here to download high resolution image](#)

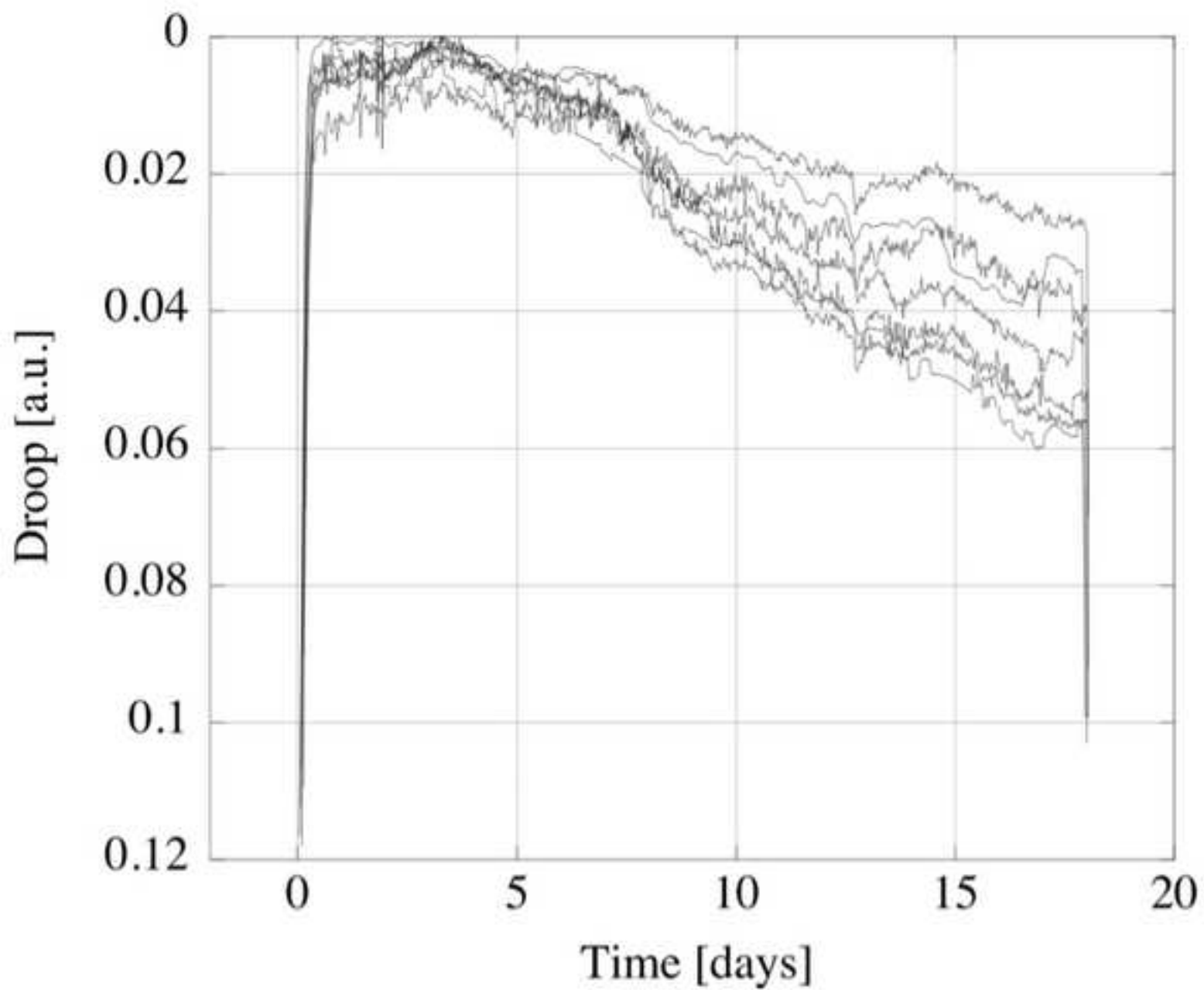


Figure 13

[Click here to download high resolution image](#)

